SINGLE PHASE GRID CONNECTED INVERTER SERVING TWO PV PANELS UNDER DIFFERENT ATMOSPHERIC CONDITIONS

A DISSERTATION

SUBMITTED IN PARTIAL FULFILLMENT OF THE REQUIREMENTS
FOR THE AWARD OF THE DEGREE

OF

MASTER OF TECHNOLOGY

IN

POWER SYSTEM

SUBMITTED BY
DHRUV BHATIA

2k18/PSY/04

Under The Supervision Of

PROF. ALKA SINGH
&
ANKITA ARORA

ELECTRICAL ENGINEERING DEPARTMENT

DELHI TECHNOLOGICAL UNIVERSITY

(Formerly Delhi College of Engineering)
Bawana Road, Delhi-110042

JULY, 2020

DEPARTMENT OF ELECTRICAL ENGINEERING

DELHI TECHNOLOGICAL UNIVERSITY

(Formerly Delhi College of Engineering)

Bawana Road, Delhi-110042

CANDIDATE'S DECLARATION

I, DHRUV BHATIA, Roll No. 2K18/PSY/04 student of M.Tech. (Power System), hereby declare that the project Dissertation titled "**SINGLE PHASE GRID CONNECTED INVERTER SERVING TWO PV PANELS UNDER DIFFERENT ATMOSPHERIC CONDITIONS**" which is submitted by me to the Department of Electrical Engineering Department, Delhi Technological University, Delhi in partial fulfillment of the requirement for the award of the degree of Master of Technology, is original and not copied from any source without proper citation. This work has not previously formed the basis for the award of any Degree, Diploma Associate ship, Fellowship or other similar title or recognition.

Place: Delhi

Date: 10-07-2020 (**DHRUV BHATIA)**

DEPARTMENT OF ELECTRICAL ENGINEERING

DELHI TECHNOLOGICAL UNIVERSITY

(Formerly Delhi College of Engineering)

Bawana Road, Delhi-110042

CERTIFICATE

I hereby certify that the major project titled "**SINGLE PHASE GRID CONNECTED INVERTER SERVING TWO PV PANELS UNDER DIFFERENT ATMOSPHERIC CONDITIONS** " which is submitted by DHRUV BHATIA, Roll No-2K18/PSY/04 ELECTRICAL ENGINEERING DEPARTMENT, Delhi Technological University, Delhi, in partial fulfilment of the requirement for the award of the degree of Master of Technology, is a record of the project work carried out by the students under my supervision. To the best of my knowledge this work has not been submitted in part or full for any Degree to this University or elsewhere.

PROF. ALKA SINGH

(PROJECT SUPERVISOR)

Professor

Department of Electrical Engineering

Delhi Technological University

ANKITA ARORA

(PROJECT CO-SUPERVISOR)

Assistant Professor

Department of Electrical Engineering

Delhi Technological University

Place: Delhi

Date: 25-08-2020

DEPARTMENT OF ELECTRICAL ENGINEERING

DELHI TECHNOLOGICAL UNIVERSITY

(Formerly Delhi College of Engineering)

Bawana Road, Delhi-110042

ACKNOWLEDGEMENT

I am highly grateful to the Department of Electrical Engineering, Delhi Technological University (DTU) for providing this opportunity to carry out this project work.

The constant guidance and encouragement received from my Project guide **Prof. ALKA SINGH** and co-guide **ANKITA ARORA** of Department of Electrical Engineering, DTU, has been of great help and inspiration in carrying my present work and is acknowledged with reverential thanks.

I would like to express a deep sense of gratitude and thanks to **Prof. ALKA SINGH** for allowing me to work in Power System laboratory to carry out this project work.

Finally, I would like to expresses gratitude to all faculty members of Electrical Engineering Department, DTU for their intellectual support in my M.tech study at DTU.

Place: Delhi

Date: 10-07-2020

DHRUV BHATIA

M.Tech (Power System)

(2K18/PSY/04)

ABSTRACT

Innovation in photovoltaic systems has been constantly increasing since its invention and integration to the power grid. The cost of generating power has been decreasing with the invention of new technologies. The control of energy has also become more dynamic. With these increasing innovations the efficiency to extract maximum solar power from a system is increasing.

In this work a single stage one phase grid tied inverter which has two serially connected PV panels as its input is designed. A transformerless single stage topology has been used which has the advantage of less weight, low volume, low complexity and less cost. The PV panels has been exposed to varied conditions of irradiance and temperature. Since the serially connected modules are only two it is easier to extract maximum power from each one and control system is also less complex. The control strategies for the synchronization of the proposed inverter topology with the power grid has been carried out using a conventional PI controller and a Fuzzy Logic controller.

A 1.5 KW model of the scheme has been simulated in MATLAB-Simulink where the PV modules are exposed to different conditions of temperature and irradiance. Bothe the PV panels are controlled separately making the control scheme as decoupled. The operation of the inverter is discussed with an in depth analysis of the control scheme with the two controllers. A comparative analysis has also been carried out using the results obtained for the Proportional Integral Controller and Fuzzy Logic Controller.

CONTENTS

LIST OF FIGURES

LIST OF TABLES

LIST OF SYMBOLS

1.	I_{ph}	Photocurrent for PV cell
2.	I_D	Diode Current for PV cell
3.	I_{sh}	Shunt Current
4.	R_s	Series Resistance of PV cell
5.	R_{sh}	Shunt Resistance of PV cll
6.	V_D	Diode Voltage
7.	I_s	Diode Reverse Saturation Current of PV cell
8.	V_T	Thermal Voltage
9.	K_B	Boltzmann constant
10.	q	Electron Charge constant
11.	N_s	Number of serially connected cells
12.	N_p	Number of parallel connected cells
13.	I_{SC}	Short Circuit Current of PV cell
14.	I_{rs}	Reverse Saturation Current of PV cell
15.	E_g	Band gap Energy
16.	V_{oc}	Open Circuit Voltage
17.	C_f	Input side DC Link Capacitor
18.	C_{o1}	Output Filter Capacitor
19.	L_1	Output Filter Inductor
20.	C_{pv}	Parasitic Capacitor
21.	P_{gco}	Total power across the grid
22.	P_{MPP}	Maximum Power Extracted from the PV Modules
23.	V_{MPP}	Maximum Voltage Extracted from the PV Modules
24.	I_{MPP}	Maximum Current Extracted from the PV Modules
25.	V_{co}	Voltage across Output Filter Capacitor
26.	I_L	Current through Output Filter Inductor
27.	I_g	Grid Current injected by the system
28.	V_{com}	Amplitude of Voltage across Output Filter Capacitor

29. D_m Amplitude of Duty Cycle for the switches

30. V_g Grid Voltage

CHAPTER 1

INTRODUCTION

1.1 BACKGROUND

The economic development of any country is very closely related to the amount of energy consumption. The development of new technologies are totally dependent on the uninterruptible supply of electricity. This supply of energy is obtained conventionally from the fossil fuels and now from the renewable energy sources such as solar, wind etc.

The coal reserves are likely to last for about 200 years and the oil and natural gas will be consumed within 25-30 years. Since these are the main sources of energy for electricity generation but these sources are available in a limited quantity and burning of these fossil fuels adds a huge amount of carbon dioxide and other harmful greenhouse gases into the atmosphere which leads to global warming and changes in the climate cycle. Therefore alternative ways for electricity generation are required. Photovoltaic Systems, Wind turbine generator, battery storage systems, hydro power are more sustainable sources of energy than the conventional Thermal Power Plants. Some of the advantages of renewable energy sources is that they are clean to environment, inexhaustible and they do not produce any greenhouse gases thus reducing the above mentioned problems.

1.1.1. Solar Energy

A Photovoltaic cell converts the energy from the sun to electrical energy. Some of the advantages of PV systems are that they have a low maintenance and operational cost. But the major problem they face is that the efficiency to convert electrical power from solar energy is very low. The also face a drawback of changing weather. The basic units of a PV panel are cells. These cells are connected in series and parallel to form a PV array. These PV arrays have a non-linear I-V characteristics. The DC voltage

generated at the output of the PV panel can be directly used for lightening systems and DC motors while most of the other applications require an inverter to convert this DC power to AC power which can either be fed directly to the grid or can be used in local linear/non-linear loads [1].

1.1.2. Solar Energy in India

India is one of the fastest developing country for solar energy. With an installed capacity of 371 GW India is amongst the top producers of electricity in the world [2]. India has initiated an International Solar Alliance which has been accepted by 121 countries. The main objective of this alliance is to reduce the dependency on fossil fuels and encourage solar energy generations amongst its members. The Government of India has also set up many schemes which encourages solar energy generation. Some of the schemes are:

1. Jawaharlal Nehru National Solar Mission (JNNSM) [3]

It is one of the 8 national missions adopted by India. The main objective of the scheme is to encourage to production of grid connected solar generation. It had a target of generating 20,000 MW of power by 2022 which was achieved much earlier and now this target has been revised to 100,000 MW in the year 2015 and again increased to 400,000 MW.

2. Government Yojana : Solar Energy Subsidy Scheme [4]

This scheme encourages the individual to install local solar panels since the government would provide subsidy if an individual has installed solar panels at rooftops. The main advantage of this scheme is to the individual itself since by installing solar panels he is able to cut down on the electricity bill and also it reduces the burden on the thermal power plants.

3. Solar Park Scheme [5]

The Ministry of New and Renewable Energy has an objective to set solar parks in many states of India with the solar park scheme. The government is planning to install 25 solar parks in India with a combined capacity of 20,000 MW [5]. As of 2019 a total of 42 solar parks have been installed in India with a total capacity of 23,000 MW. These 42 solar parks have been installed in 17 Indian states.

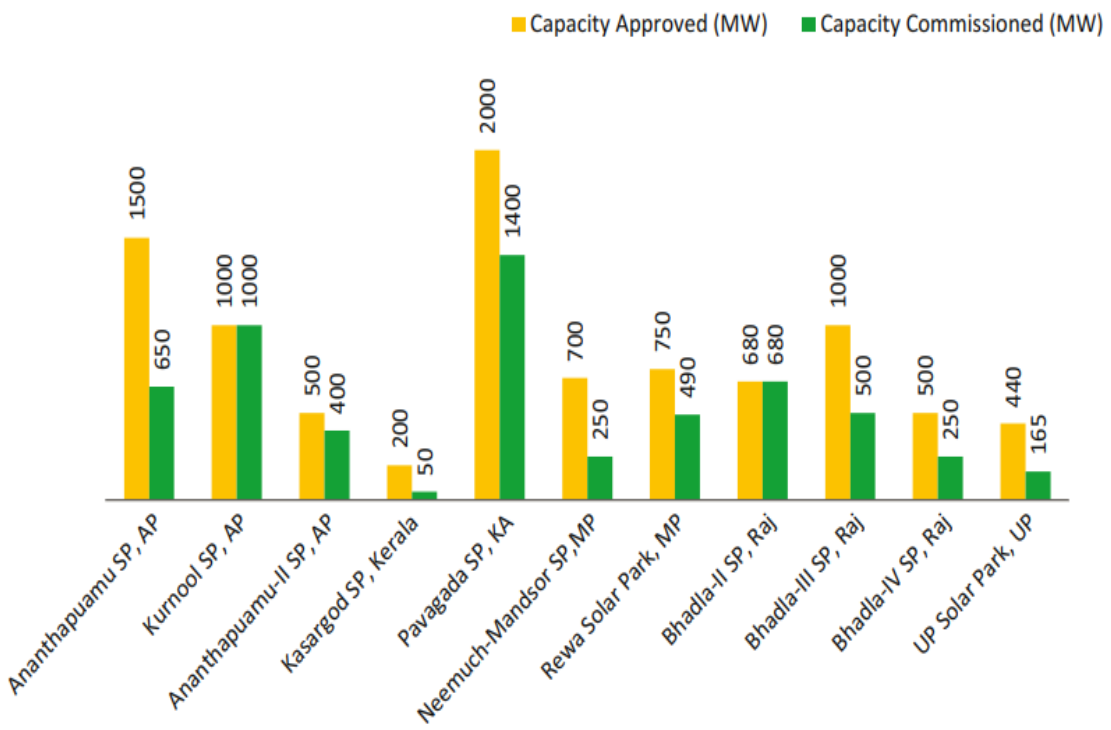

Fig. 1.1. Solar Parks commissioned in India (as on March 2019)

4. UDAY Scheme [6]

The scheme aims at reforming the power sector, lowering the cost of generation, encouraging generation of solar energy and improve the current condition of the power companies of the country. The scheme came as a revival package for the distribution companies which were having huge losses.

5. Rooftop Scheme [6]

This scheme was executed by SECI to initiate the installation of rooftop solar panels. The scheme has initiated rooftop solar generation in CPWD for 50 MW and 75 MW for warehouses.

The year wise solar capacity installed in India from 2008 to 2019 is depicted in the bar chart below. It shows a good growth in the installed capacity. All the values have been taken in MW.

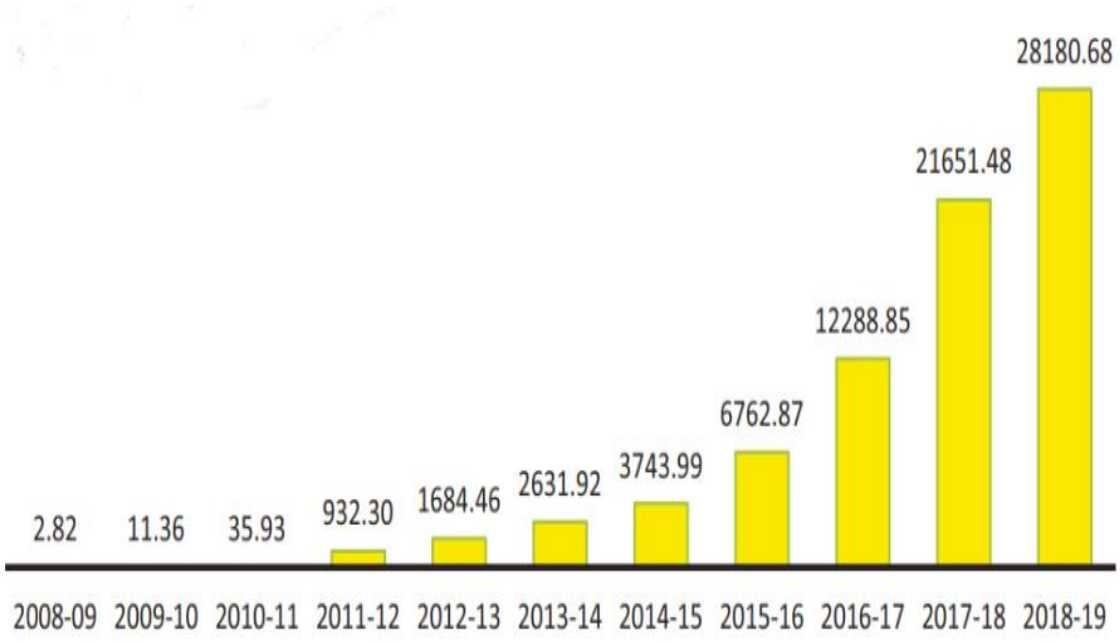

Fig. 1.2. Cumulative Capacity of Installed Solar Power : Year wise (in MW,as on March 2019)

The state wise solar capacity installed in India till March 2019 is shown in the bar chart below. All the values has been taken in MW.

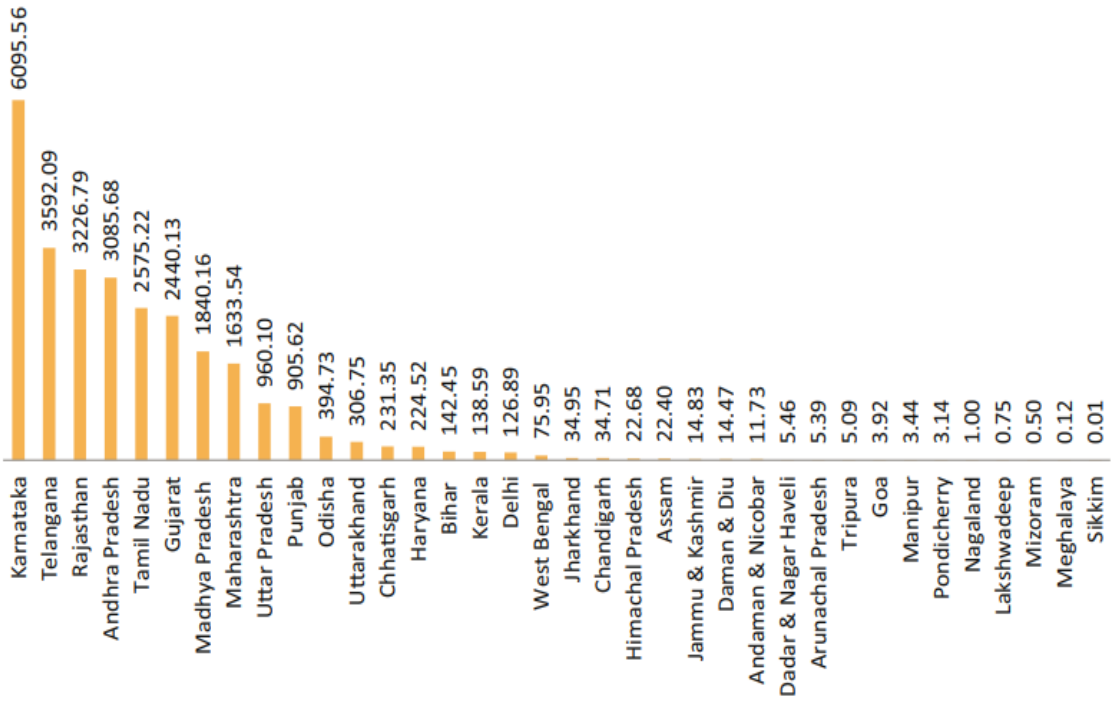

Fig. 1.3. State wise Capacity of Installed Solar Power (in MW, as on March 2019)

1.1.3 Grid Connected System

The grid connected systems can be divided into two major categories i.e. Single Stage and Multi-stage systems. In the multi-stage system the power flow from the PV array to the grid is divided into two stages. In the first stage the PV array DC voltage is boosted (increased) and maximum power point is tracked. This stage is comprised of a boost or buck-boost DC-DC power electronic converter topology. The second stage consists of an inverter which converts DC power to AC. While this technique is time tested and work very well but they suffer from the drawbacks such as high cost, low efficiency, large size [7].

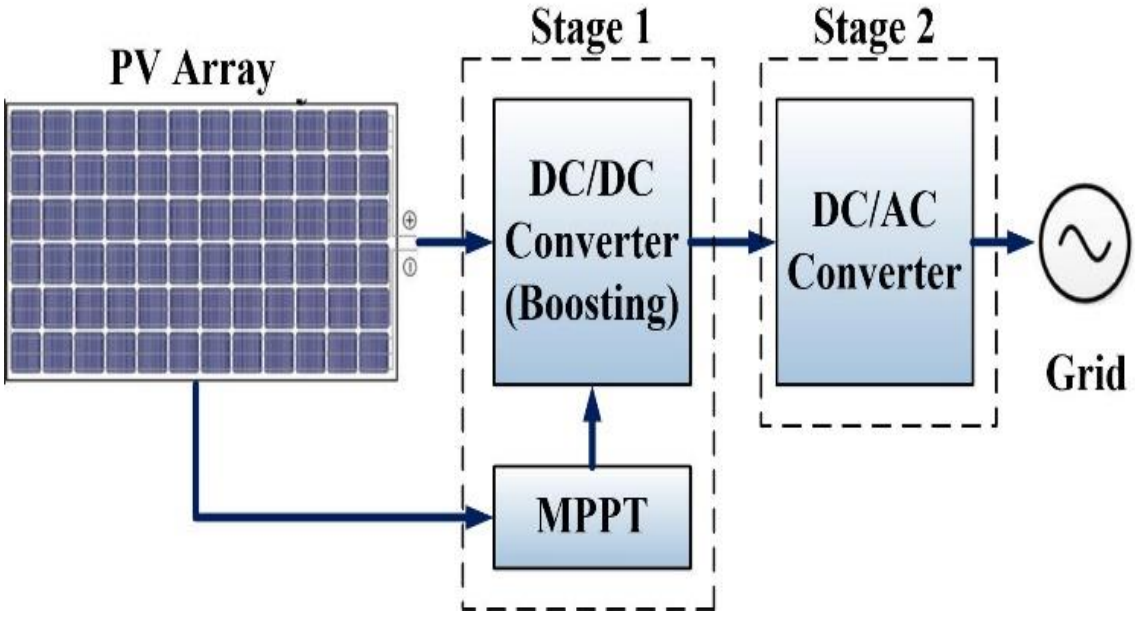

Fig. 1.4. Dual Stage PV System

Since the multi-stage systems suffer from the above mentioned drawbacks the simple solutions can be:

1. To only use the inverter stage i.e. H-bridge inverter with transformer [8].

2. Using a PV array with large output voltage with a H-bridge inverter [9][10].

These options have the drawback that they are bulky and increases the total cost of the system and large PV arrays suffers from creation of hotspots and increased leakage current from the parasitic capacitor[11][12].

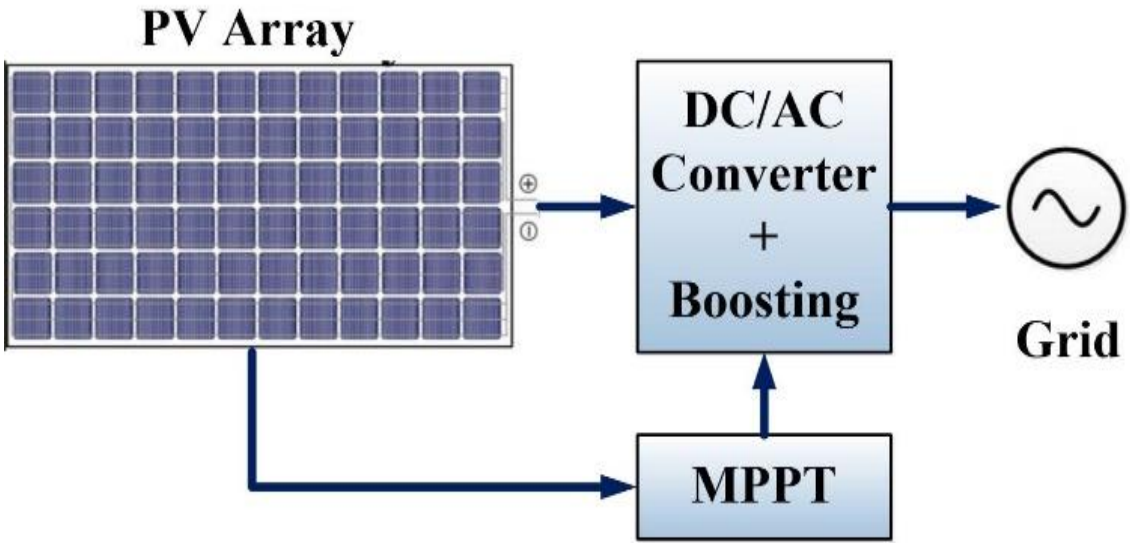

Fig. 1.5. Single Stage PV System.

1.2 THESIS FORMULATION

The outlines of this thesis is as follows:

Chapter 1: The basic introduction of Solar Energy and why it is necessary for power generation in the coming years. The schemes undertaken by the Government of India to encourage solar power generation. Various statistics have been shown for the recent trends and scenario of solar power in India. In the end a brief description about the grid connected PV systems with single stage and multi stage systems has been described.

Chapter 2: This chapter deals with the basic components of the grid connected PV systems. Firstly an introduction to the PV cell has been described with various PV models and its derivation then various MPPT schemes has been discussed, the MPPT scheme plays a very important role to extract the maximum power from the PV panel and thus increasing the efficiency of the system. After this single phase transformerless inverters for grid connected systems has been reviewed. The advantages and disadvantages of each topology has been discussed. In the end the PWM schemes for generating the gating pulses has been discussed.

Chapter 3: In this chapter the proposed inverter operation and modelling has been taken into account. The inverter topology with various modes of operation and its switching states is described. The small signal modelling has also been derived from [32]. The

selection criteria of various passive elements of the scheme has also been explained in this chapter.

Chapter 4: This chapter describes the control strategy for the proposed inverter using a Conventional PI controller as described in [32] [34]. Results have been obtained for the input side PV module parameters and the output side grid current and voltages.

Chapter 5: In this chapter the conventional PI controller has been replaced by the Fuzzy Logic Controller (FLC) for the control scheme. Improved results have been obtained from the conventional control strategy with the decrease in THD% for the injected grid current.

Chapter 6: This chapter included the conclusion and the future work on this work.

CHAPTER 2

GRID CONNECTED PV SYSTEM

2.1. PHOTOVOLTAIC SYSTEM

2.1.1. Photovoltaic Effect

PV effect is the process of conversion of sunlight to direct current electricity. Two semiconductors generally made of silicon are used to form a junction. This junction formed is known as the p-n junction. The two semiconductors used to form the p-n junction are made of n-type and p-type semiconductors. The n-type semiconductor is formed by doping trivalent impurity and similarly the p-type semiconductor is formed by doping pentavalent impurity [13].

The movement of excess electrons takes place from n-type to p-type through the junction while the movement of excess holes takes place from p-type to n-type semiconductor. This forms an electric field at the junction due to the formation of n-type and p-type area [14]. When the photons from the sun with energy greater than the energy of band gap of the material falls on the PV cell, electron-hole pairs are created. The electrons starts to travel in the circuit according to the electric field present at the junction of the cell. The electrons completes the circuit and then recombine with the holes. This movement of electrons creates the direct current.

2.1.2. Types of Photovoltaic Cells

PV cells used in the traditional PV panels are classified into two types i.e. Mono-crystalline and Multi-crystalline. Mono-crystalline has the advantage of better efficiency but the drawback of higher manufacturing cost [15]. While the multi-crystalline cells are

of lower quality since they contain gain boundaries which reduces the cell efficiency to great extent by introducing boundary losses [16].

2.1.3. SOLAR SPECTRUM

The solar irradiation incident on the atmosphere is varied from the irradiation on the ground. This change in irradiation takes place due to the geographic location, weather, pollution levels, climatic changes and changes in the day as well [17]. To standardize the measuring the American Society for Testing and Materials has a standardized coefficient for air mass.

The coefficient is defined as a ratio: the real sunlight path length from the atmosphere to the surface, relative to the virtual normalized path length at the zenith. So when the sun is directly over the head the coefficient is 1 and can be taken as AM1. In the mid or temperate latitudes the coefficient is taken as AM1.5. Here AM1.5 is the standard testing condition with 1 KW/m^2 taken as irradiance and room temperature as 25° C.

2.1.4. Photovoltaic Cell Models

A PV cell model can be derived by two methods which is based on their equivalent circuit: the single diode model (SDM) and the double diode model (DDM). These models are divided on the number of distinguished diodes used in the model circuit. The resistances for the shunt and series part is modelled to show the parasitic power losses.

2.1.4.1. The Single Diode Model (SDM)

The SDM is categorized into: the ideal single diode model (ISDM), the regular single diode model (RSDM) and the simplified single diode model (SSDM). The ISDM is least complex and has only 3 parameters [18]. But the main drawback of ISDM is that it does not promise good simulation results. RSDM provides better accuracy than the ISDM but this requires to solve for 5 equations because of the addition of series and shunt resistances [19]. The SSDM neglects the shunt resistance to reduce the complexity for modelling but suffers from inaccurate results with varying insolation and temperatures [20].

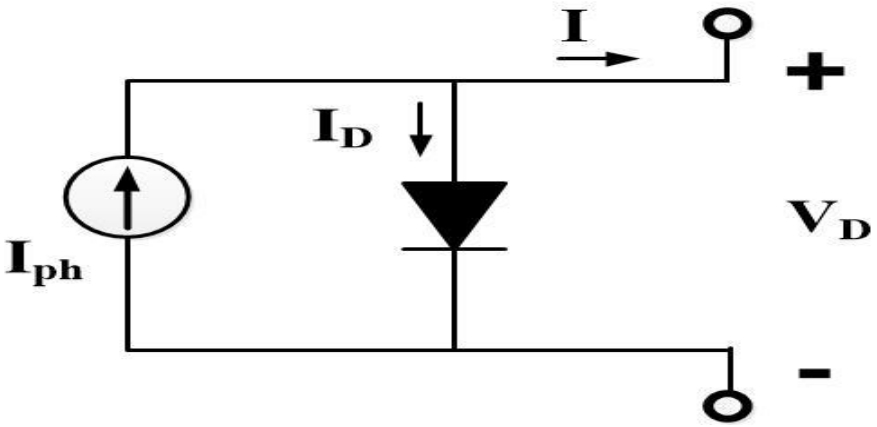

Fig. 2.1. Ideal Single Diode Model (ISDM)

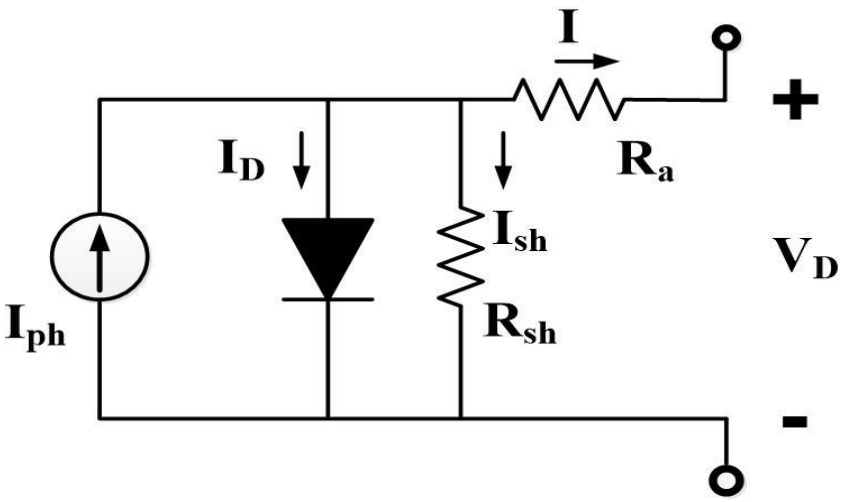

Fig. 2.2. Regular Single Diode Model (RSDM)

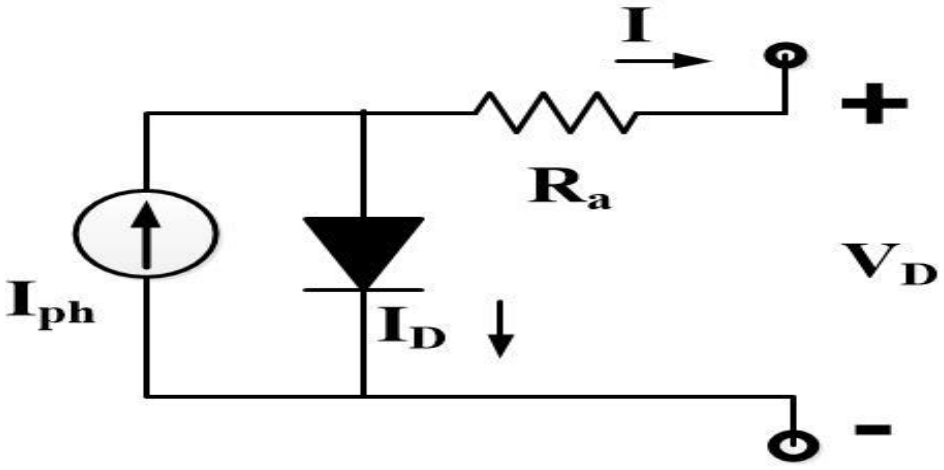

Fig. 2.3. Simplified Single Diode Model (SSDM)

The equations given below are derived using Regular Single Diode Model (RSDM). Using Kirchoff's Current Law:

$$I = I_{ph} - I_D - I_{sh} \tag{2.1}$$

where I_D is the diode current, I_{sh} is the shunt current and I is the total output current.

Using Kirchoff's Voltage Law:

$$V_D = V + I * R_s \tag{2.2}$$

where V is the output voltage, R_s is the shunt resistance and V_D is the diode voltage.

Using Ohm's Law:

$$V_D = I_{sh} * R_{sh} \tag{2.3}$$

here resistance is the shunt resistance.

Substituting Eq. (2.3) in Eq. (2.2):

$$I_{sh} = \frac{V_D}{R_{sh}} = \frac{V+IR_s}{R_{sh}} \tag{2.4}$$

From the Shockley's Diode Equation we have:

$$I_D = I_s[e^{\frac{V_D}{nV_T}} - 1] \tag{2.5}$$

The thermal voltage is expressed as:

$$V_T = \frac{k_B * T}{q} \tag{2.6}$$

here T is the temperature of the cell, k_B is the Boltzmann constant and q is the electron charge constant.

Substituting Eq. (2.4) to (2.6) into Eq. (2.1), we will have the final form of the I-V characteristics equation for a single PV cell using the RSDM:

$$I = I_{ph} - I_s\left(e^{\left(\frac{V+IR_s}{nV_T}\right)} - 1\right) - \frac{V_D+IR_a}{R_{sh}} \tag{2.7}$$

2.1.4.2. The Double Diode Model (DDM)

The double diode model has the advantage of better accuracy than the regular single diode model but it has a drawback of increased complexity. The recombination losses in the depletion region are not neglected in this model and hence the results are more accurate [21].

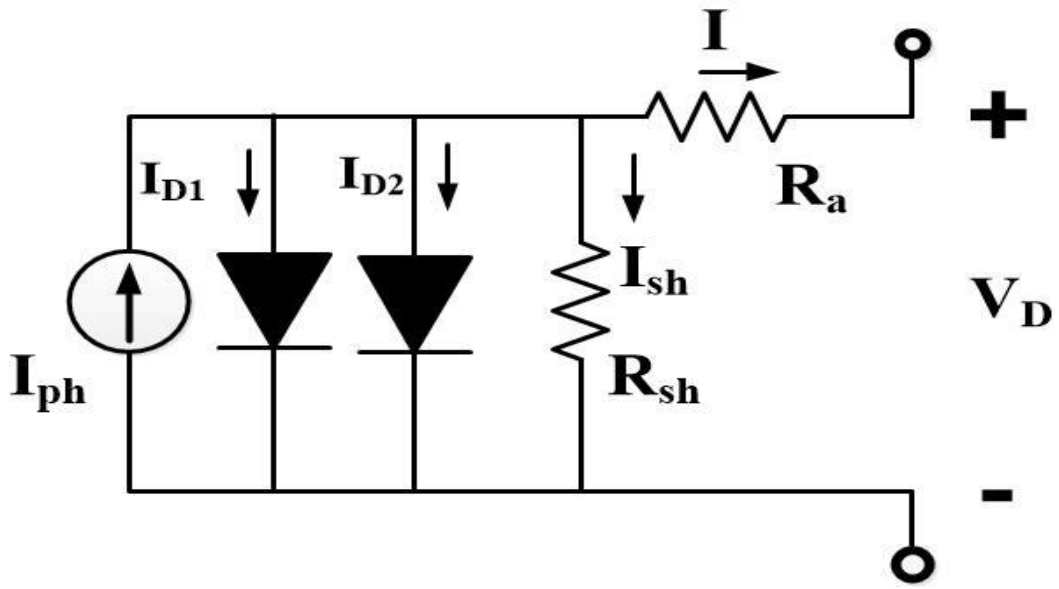

Fig. 2.4. Double Diode Model (DDM)

Using the equivalent circuit the current-voltage characteristics can be obtained by the equation:

$$I = I_{ph} - I_{D1} - I_{D2} - \frac{V+IR_s}{R_{sh}} \tag{2.8}$$

The diode currents are given below:

$$I_{D1} = I_{s1}[e^{\frac{V_D}{nV_T}} - 1] \tag{2.9}$$

$$I_{D2} = I_{s2}[e^{\frac{V_D}{nV_T}} - 1] \tag{2.10}$$

The simulation studies needs some more equations to be derived which are given as follows:

The equation for the PV array with N_s as the number of serially connected cells and N_p as the number of parallel connected cells can be derives similar to Eq. (2.7) as:

$$I = N_p I_{ph} - \frac{N_p I_{ph}}{\left[e^{\frac{V_D}{nV_T}} - 1\right]}\left[e^{\frac{\frac{V}{N_s}+\frac{IR_s}{N_p}}{nV_T}} - 1\right] - \frac{\frac{N_p}{N_s}V + IR_s}{R_{sh}} \quad (2.11)$$

The photocurrent equation is to calculate the photocurrent generate by the PV cell(s) based on the solar radiation it absorbs and the operating temperature of the device.

$$I_{ph} = [I_{sc} + K_i(T - 298)]\frac{I_{rr}}{1000} \quad (2.12)$$

The reverse saturation current is given as,

$$I_{rs} = \frac{I_{sc}}{[e^{(\frac{V_{oc}}{nN_sV_T})} - 1]} \quad (2.13)$$

$$I_s = I_{rs}(\frac{T}{T_r})^3 e^{[qE_q\frac{\left(\frac{1}{T_r}-\frac{1}{T}\right)}{nk}]} \quad (2.14)$$

Now the equation to model the diode current in a PV array with N_s as the number of series cells and N_p as the number of parallel cells is given as

$$I_D = I_s[e^{\frac{\frac{V}{N_s}+\frac{IR_s}{N_p}}{nV_T}} - 1] \quad (2.15)$$

2.1.5. Output Characteristics of a PV Module

The following parameters are used to plot the I-V characteristics and P-V characteristics of the PV module.

PARAMETER	**VALUE**
V_{oc}	270 V
I_{sc}	3.58 A
Voltage at MPP (V_{mp})	217 V
Current at MPP (I_{mp})	3.52 A
Parallel Strings	2
Series Connected Modules per String	10
Cells per Module	60
Maximum Power of the Subarray	780 W

Table 2.1. Parameters for PV Subarrays

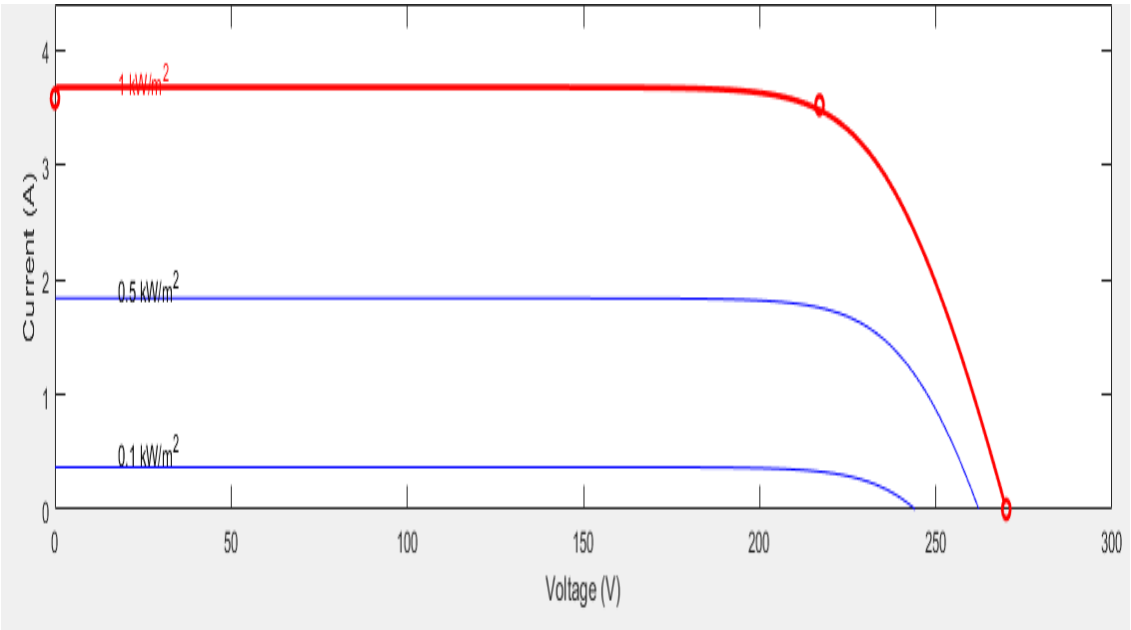

Fig. 2.5. Current-Voltage Characteristics of PV Module

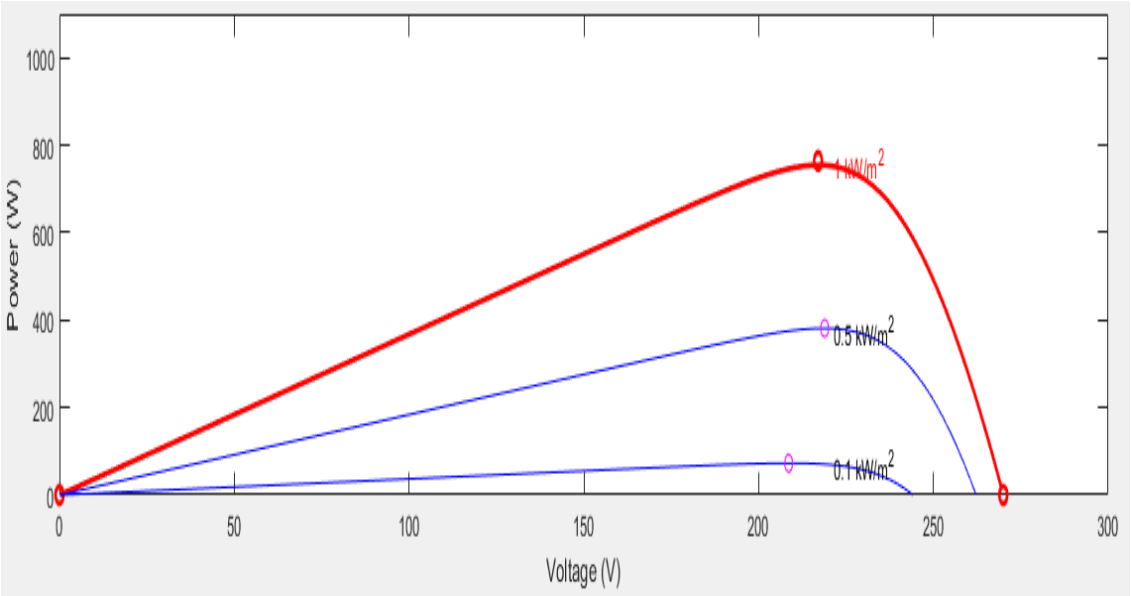

Fig. 2.6. Power-Voltage Characteristics of PV Module

2.2. Maximum Power Point Tracking (MPPT)

The non-linear characteristics of a PV module changes with the variation in irradiance and temperature levels. The electric power output of the PV module depends on this sun's

intensity and the atmospheric temperature. Since the PV arrays are expensive to made, it is highly necessary that the maximum power must be extracted from it at any given operating condition. This will increase the total usage of the solar energy thus increasing the efficiency of the system. The MPPT algorithms thus find the point of maximum power at the P-V characteristics of the subarray at a particular operating condition. Ideally the MPPT algorithm should change this operating point with minimum time when there is a change in the operating conditions [22].

Some of the MPPT algorithms are discussed below:

2.2.1. Perturb and Observe (P&O)

Perturb and Observe algorithm is straightforward, the past information of the PV voltage and current is not required and also it does not depend on the irradiance and the temperature of cell therefore it is easy to realise the algorithm for practical uses. It perturbs the operating point of the system causing the PV array terminal voltage to fluctuate around the MPP voltage even if the solar irradiance and the cell temperature are constants [23].

P&O algorithm has the advantage of reduced complexity but it has a drawback of reduced speed and accuracy. The reduced accuracy is obtained in transient period calculations when the speed of the algorithm needs to be very fast. The selection of the parameters of the algorithm is also very difficult to achieve [24].

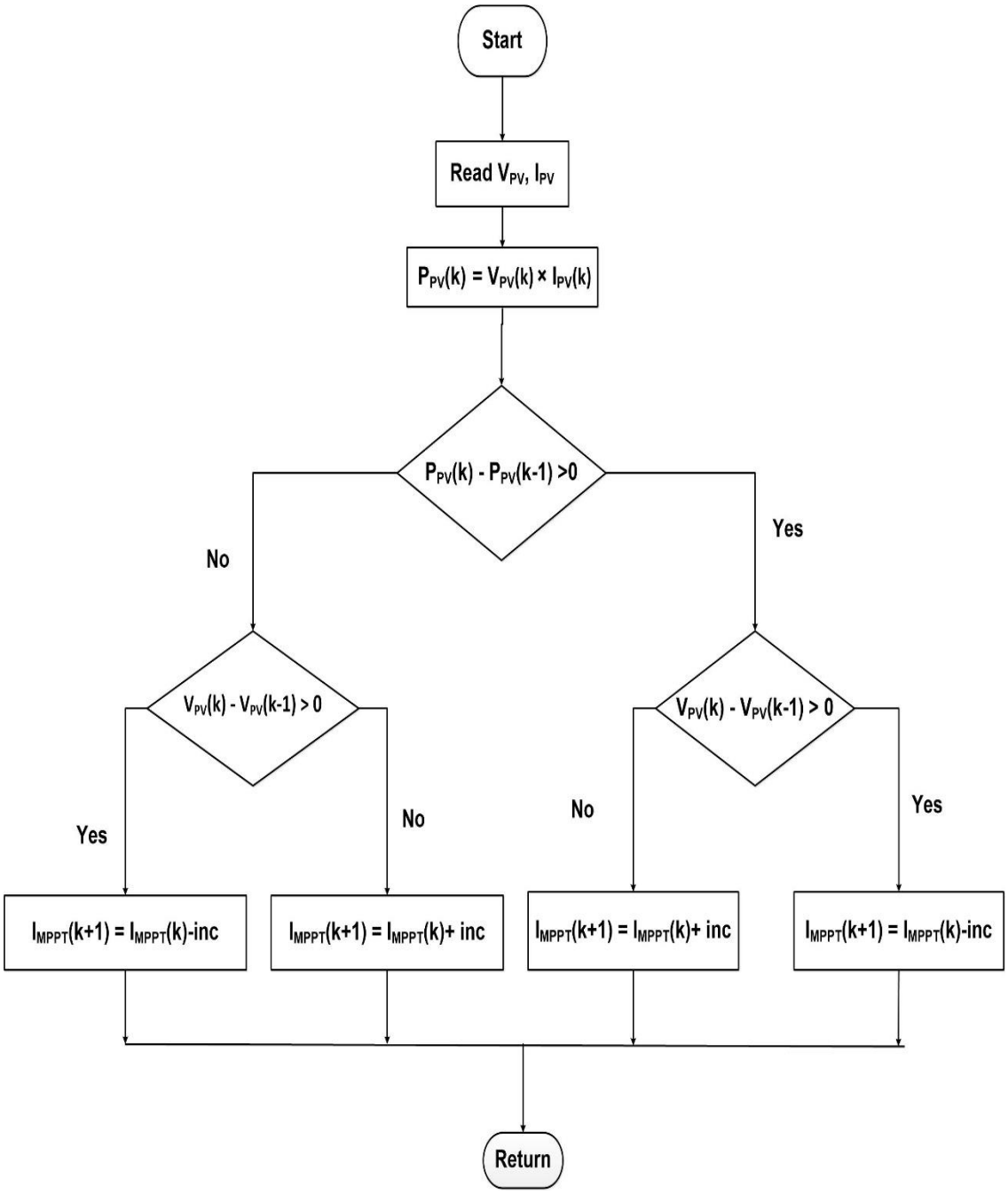

Fig. 2.7. P&O MPPT Algorithm

2.2.2. Incremental Conductance

Incremental conductance looks into the fact of the output characteristics of the PV subarrays that at the maximum power point of the system the slope of the P-V characteristics is zero. It is given as:

$\Delta P/\Delta V = 0$ at MPP with $P=VI$

Since,

$$\frac{dP}{dV} = \frac{d(VI)}{dV} = I + V\frac{dI}{dV} \cong I + V\frac{\Delta I}{\Delta V} \quad (2.16)$$

$$\frac{\Delta I}{\Delta V} = -\frac{I}{V}, \quad \text{if P = MPP} \quad (2.17)$$

$$\frac{\Delta I}{\Delta V} > -\frac{I}{V}, \quad \text{if P < MPP} \quad (2.18)$$

$$\frac{\Delta I}{\Delta V} < -\frac{I}{V}, \quad \text{if P > MPP} \quad (2.19)$$

The Maximum Power Point is tracked by comparing the instantaneous conductance with the incremental conductance. This algorithm is fast and requires high sampling rates. It has the advantage of better performance on varying conditions, it is fast and more accurate. The only drawback of the algorithm is that its implementation difficult in control systems but with using microcontrollers it has become easier to implement this algorithm [25].

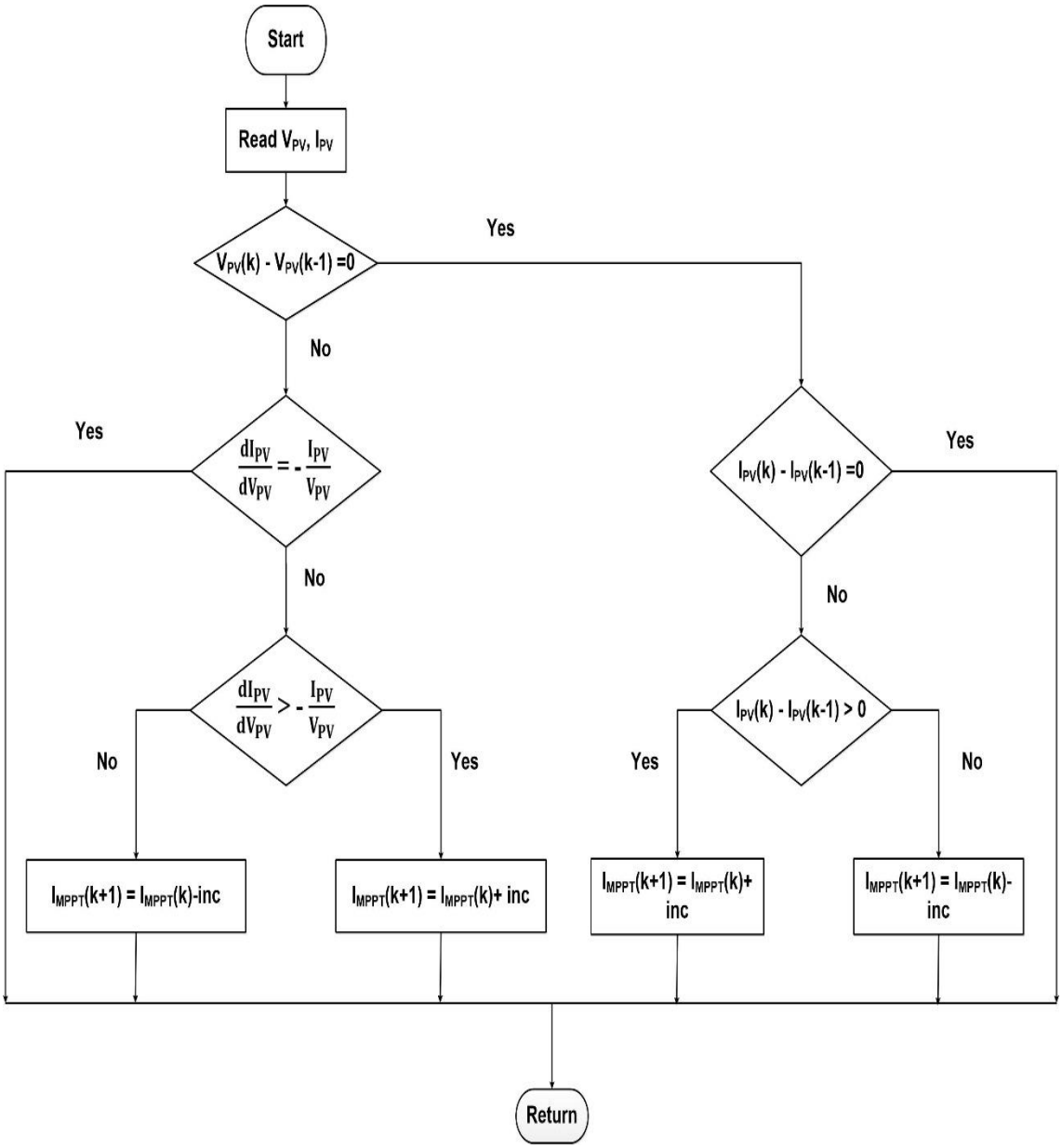

Fig. 2.8. Incremental Conductance MPPT Algorithm

2.2.3. Ripple Correlation

Under unity power factor the grid voltage and current are in phase with each other. The instantaneous power is given by the expression:

$$P_{grid}(t) = V_{grid} * I_{grid}(1 + \cos(2wt)) \quad (2.20)$$

The instantaneous power is at the double frequency than the voltages and currents. This makes the ripple also included in the DC side of the system. Hence the behaviour of the PV voltage and power ripple is used to compute the MPP of the subarray [22].

The average term of the instantaneous power terms are used to calculate the correlation terms.

$$P'_{PV} = P_{PV} - P_{avg} \tag{2.21}$$

$$V'_{PV} = V_{PV} - V_{avg} \tag{2.22}$$

dP is the function of the product of the above two equations.

1. If dP>0 the current operating point is on the left side of the MPP.

2. If dP<0 the current operating point is on the right side of the MPP.

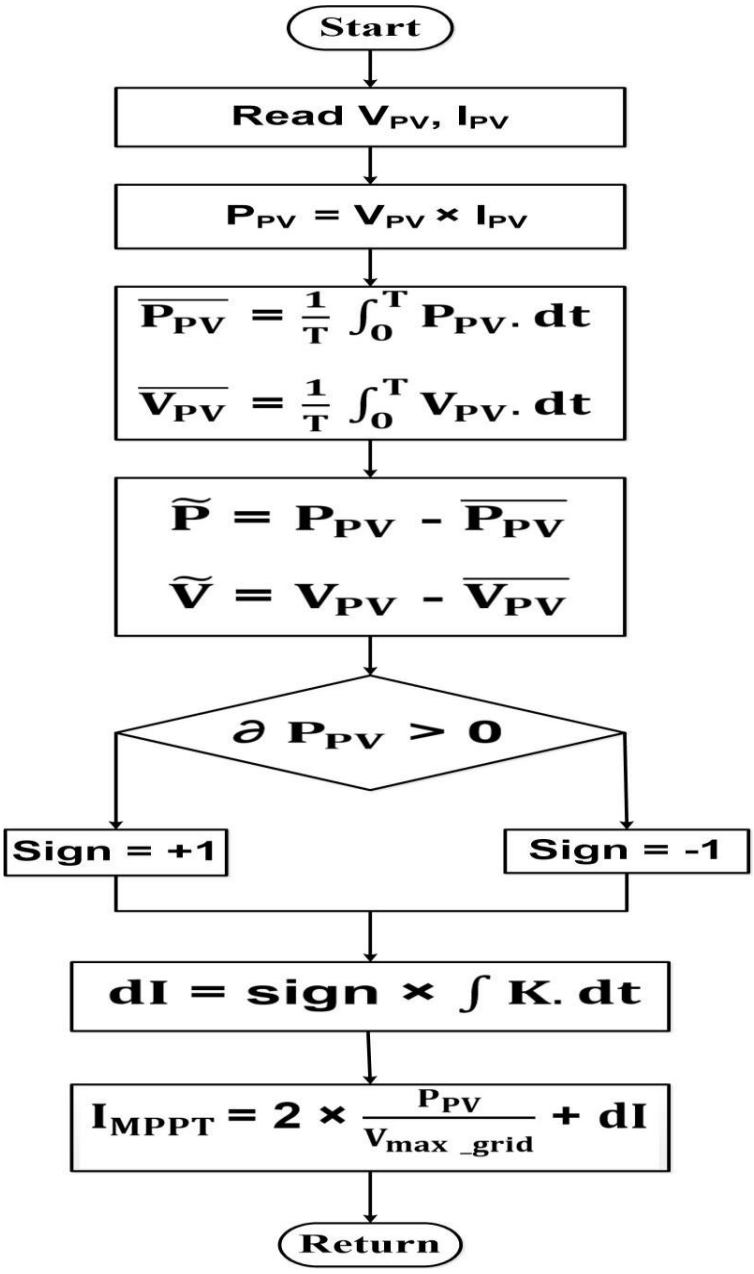

Fig. 2.9. : Ripple Correlation MPPT Algorithm

2.2.4. Temperature Method

This method unites the advantages of Constant Voltage and Incremental Conductance methods. The constant voltage method is simple and the IC method is accurate and fast, the temperature method has both these advantages. Here a temperature sensor is used instead of a current sensor. The basic operational principle of this algorithm is that the output PV voltage is proportional to the temperature of the PV module [26]. This can be shown by:

$$V_{mpp}(T) = V_{mpp}(T_{ref}) + u_{vmpp}(T - T_{ref}) \quad (2.23)$$

From the above equation it is clear that the maximum power voltage is dependent of the temperature of the PV module. The flowchart of this technique is given be

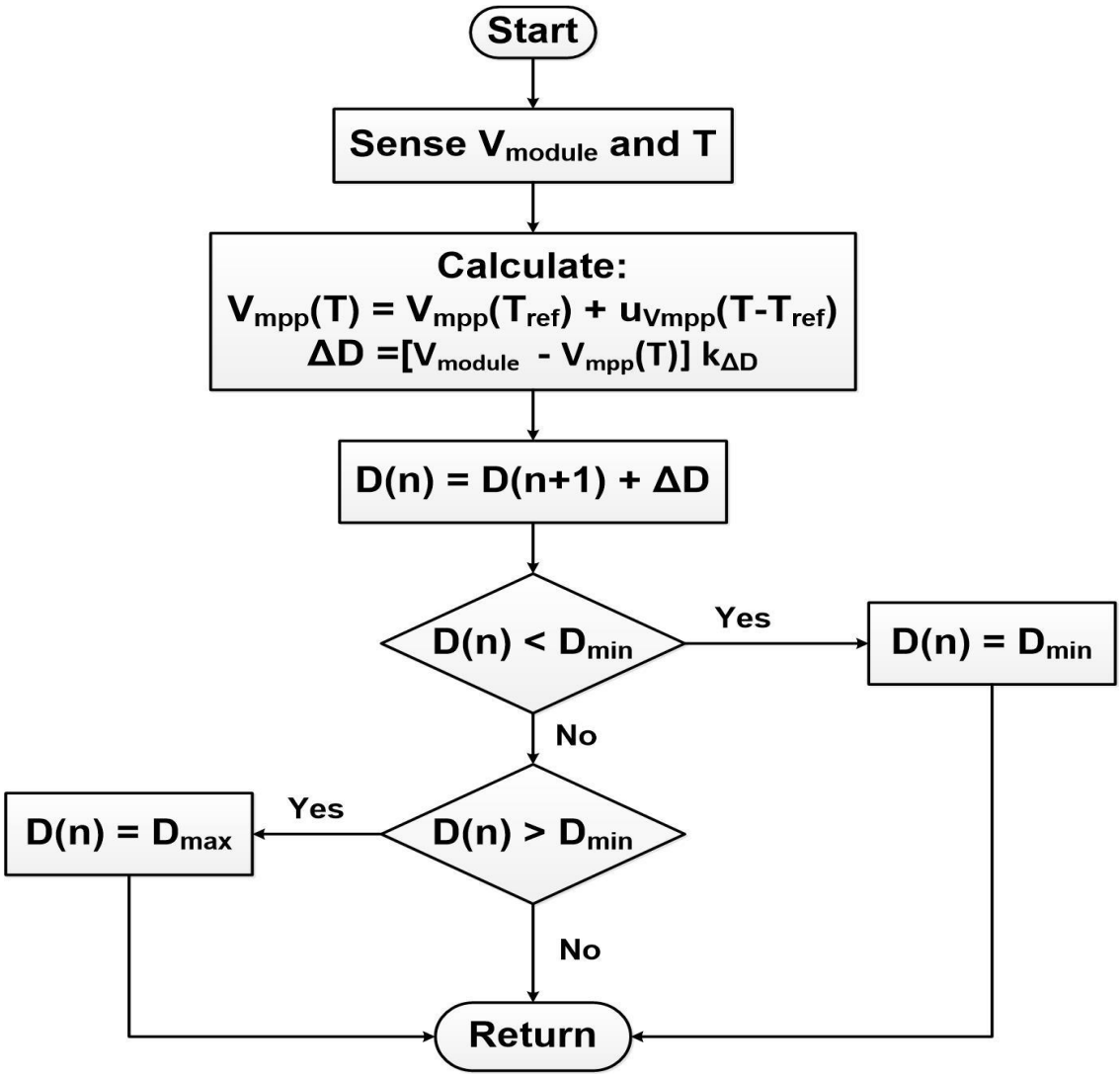

Fig. 2.10. Temperature Method MPPT Algorithm

2.3. INVERTER TOPOLOGIES

The grid-tied inverters acts as an interface between solar PV array and the utility. The transformerless inverters has become popular in the recent times in single phase systems because of their compact size, low cost and higher efficiency. However there is a leakage current issue in transformerless inverters but this can be improved by the inverter topologies and the modulation techniques.

The topologies can be classified in three ways based on their leakage current performance and decoupling method [27].

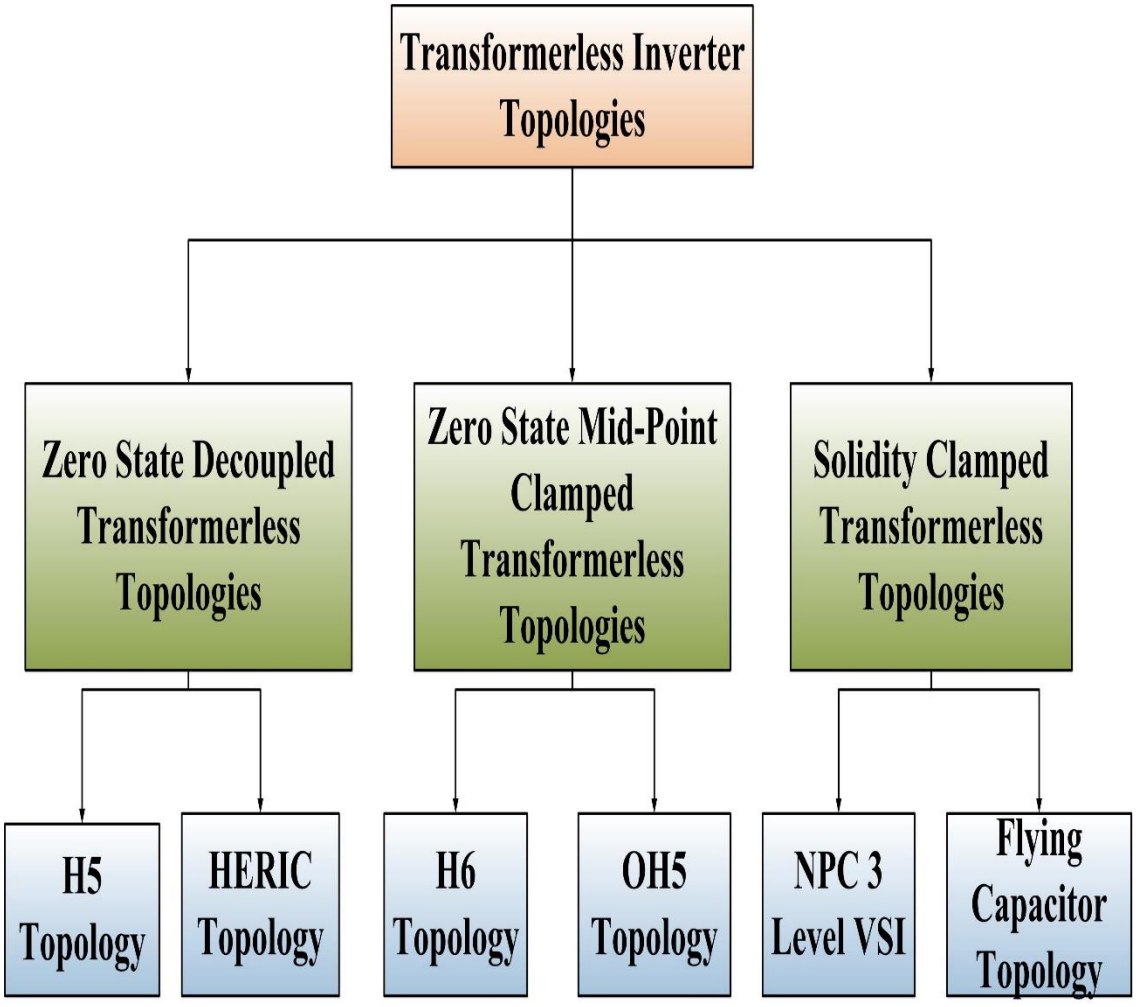

Fig. 2.11. Classification of Single Phase Transformerless Inverter Topologies [27]

2.3.1. Zero State Decoupled Transformerless Topologies

2.3.1.1. H5 Topology [28]

This topology has been developed by the world-famous company proving PV inverters i.e. SMA Solar Technology [28]. This is developed by adding an extra switch S_5 with the conventional FB topology. In PHC the switches S_1, S_4 and S_5 are switched on. This is also called the active state of the inverter.

The zero voltage is achieved when the switch S_1 and the body diode of switch S_3 are turned on. In the NHC the switches S_2, S_3 and S_5 are turned on while the freewheeling state is achieved by switching S_3 and body diode of S_1. Since three switches are turned on in the active state the switching losses are higher for this scheme. The maximum efficiency has been reported as 98.5% with this topology for 8 KW inverters.

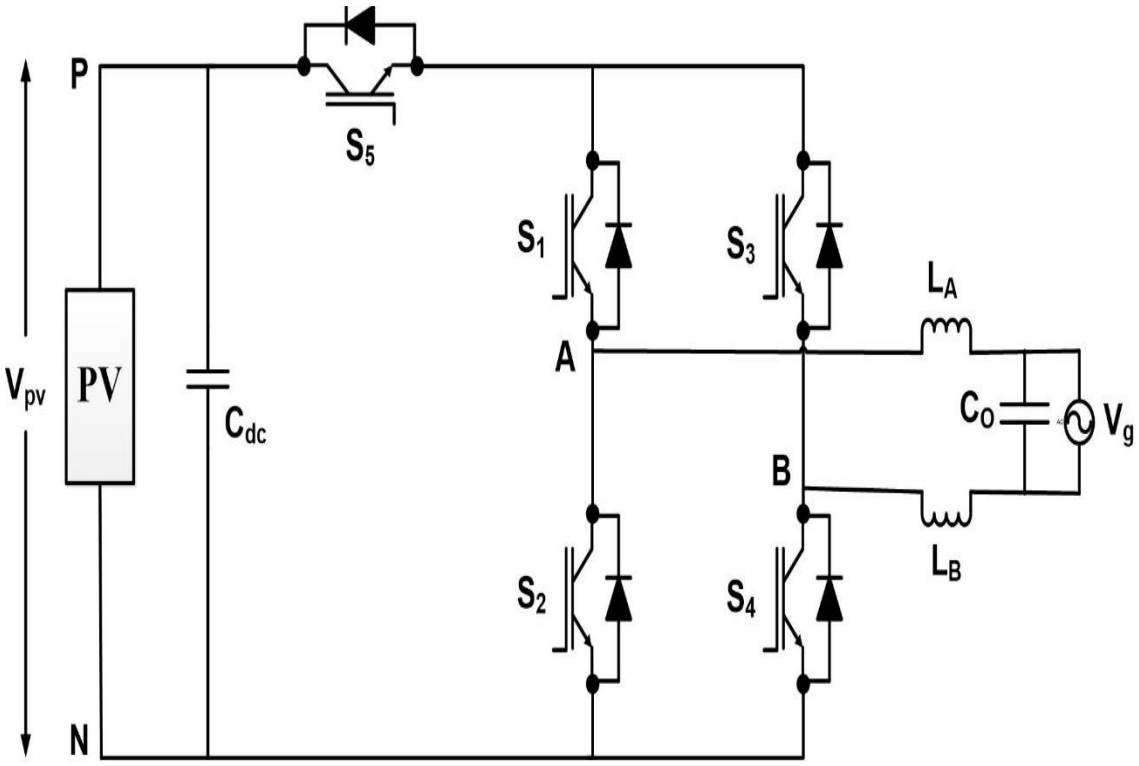

Fig. 2.12. H5 Topology

2.3.1.2. HERIC Topology [29]

The full bridge inverter with AC bypass is known as the Highly Efficient and Reliable Inverter Concept (HERIC). This topology has been used by the Sunway inverter. The two switches are added in the AC side for the freewheeling period.

The ground leakage current is minimum in this topology therefore increasing the efficiency. The efficiency is also increased since the load current also flows in the freewheeling period by switches S_5 and S_6.

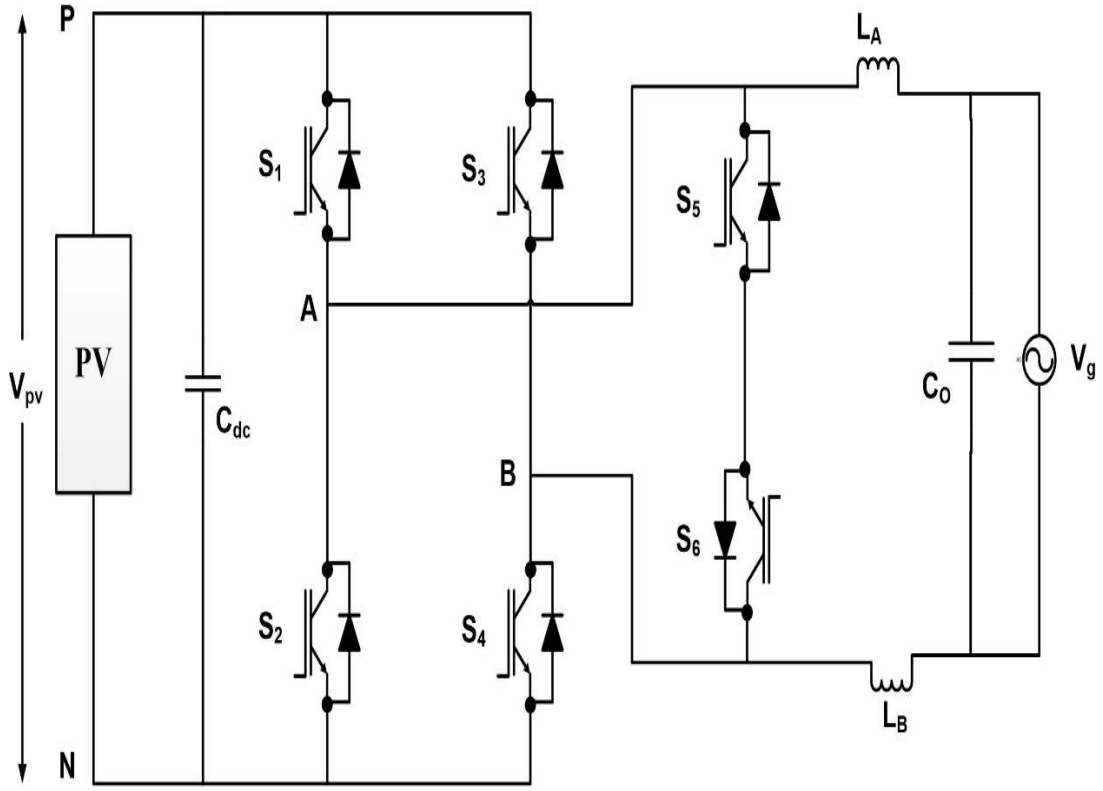

Fig. 2.13. HERIC Topology

2.3.2. Zero State Mid-Point Clamped Transformerless Topologies [27]

2.3.2.1. H6 Topology [30]

This topology can also be termed as full bridge topology with DC bypass. The switches S_1 and S_4 are used in the PHC and S_2 and S_3 are used in the NHC. In the freewheeling mode one of the two diodes are switched on based on the DC link voltage.

In this topology the leakage current only depends on the turn on speed of the diodes. Since the inductor current flows through the switches the switching losses are more in this topology with an efficiency of 97.8% for a 5 KW inverter with 350 V as DC link voltage.

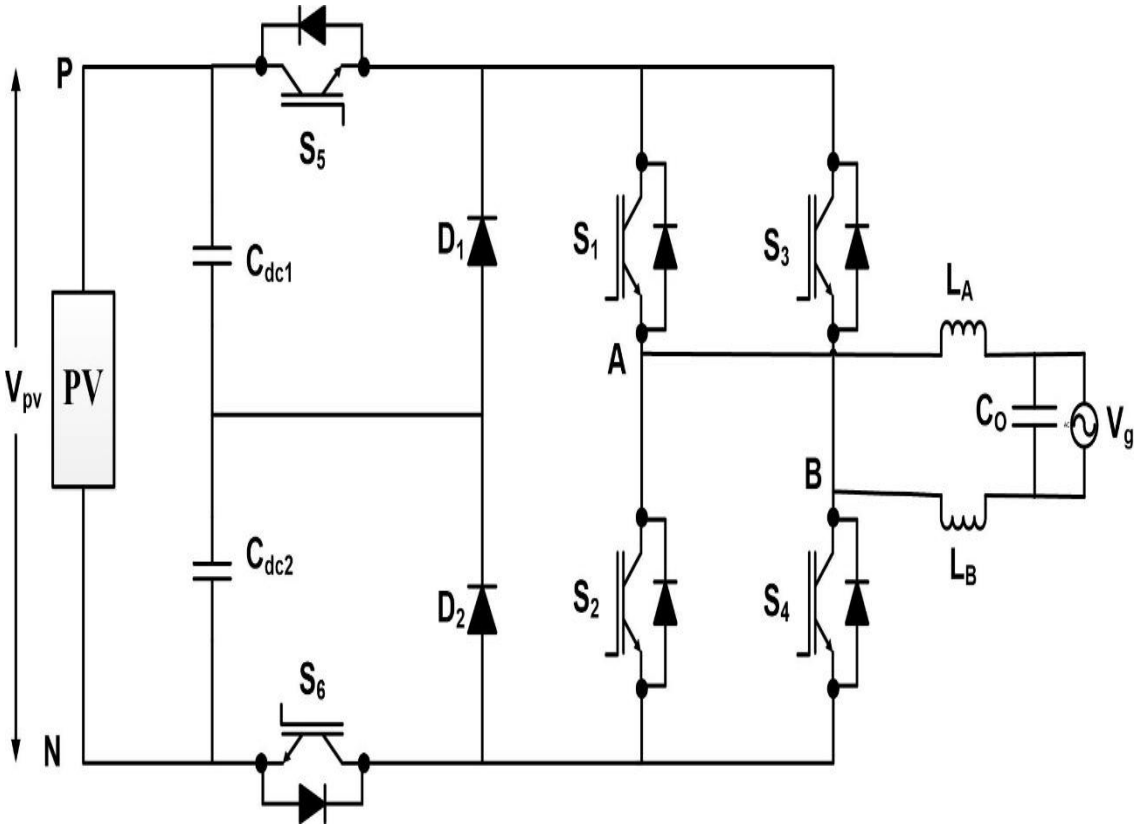

Fig. 2.14. H6 Topology

2.3.2.2. OH5 Topology [31]

This is the optimised H5 topology. A capacitor divider and a switch is consisted in the clamping branch. This topology ensures that the freewheeling potential is not more than half of the DC link voltage. Switches S_5 and S_6 are turned on simultaneously therefore a delay must be provided in the gating pulse of the two switches to avoid any short circuit condition.

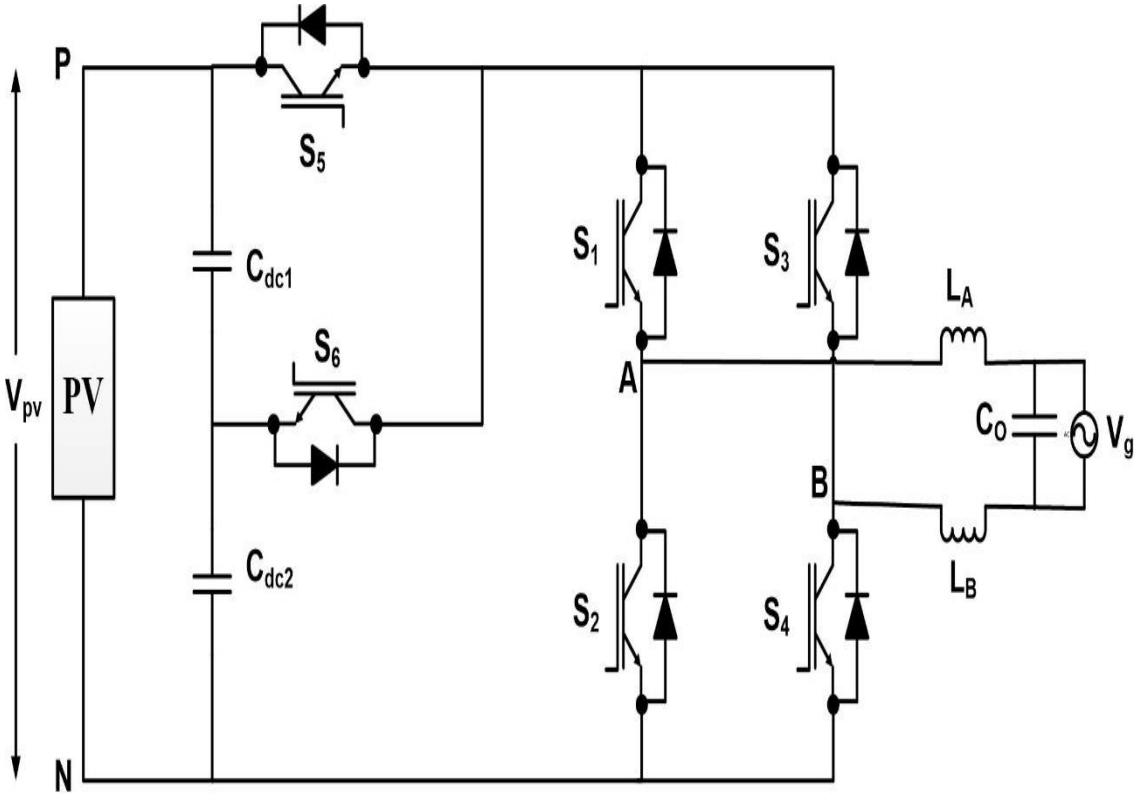

Fig. 2.15. OH5 Topology

2.3.3. Solidity Clamped Transformerless Topologies [27]

2.3.3.1. Neutral Point Clamped Three Level VSI [32]

This is a multi-level topology which is used for single phase applications where high voltages can be used. It consists of a one leg of 4 switches with two diodes clamped to the midpoint voltage. The clamping diodes are used for the freewheeling part.

This topology is similar to the H-bridge topology but it has a better performance that H-bridge. The current ripple is also less for this topology. The only drawback of this topology is that it requires high DC voltage to function with a good efficiency.

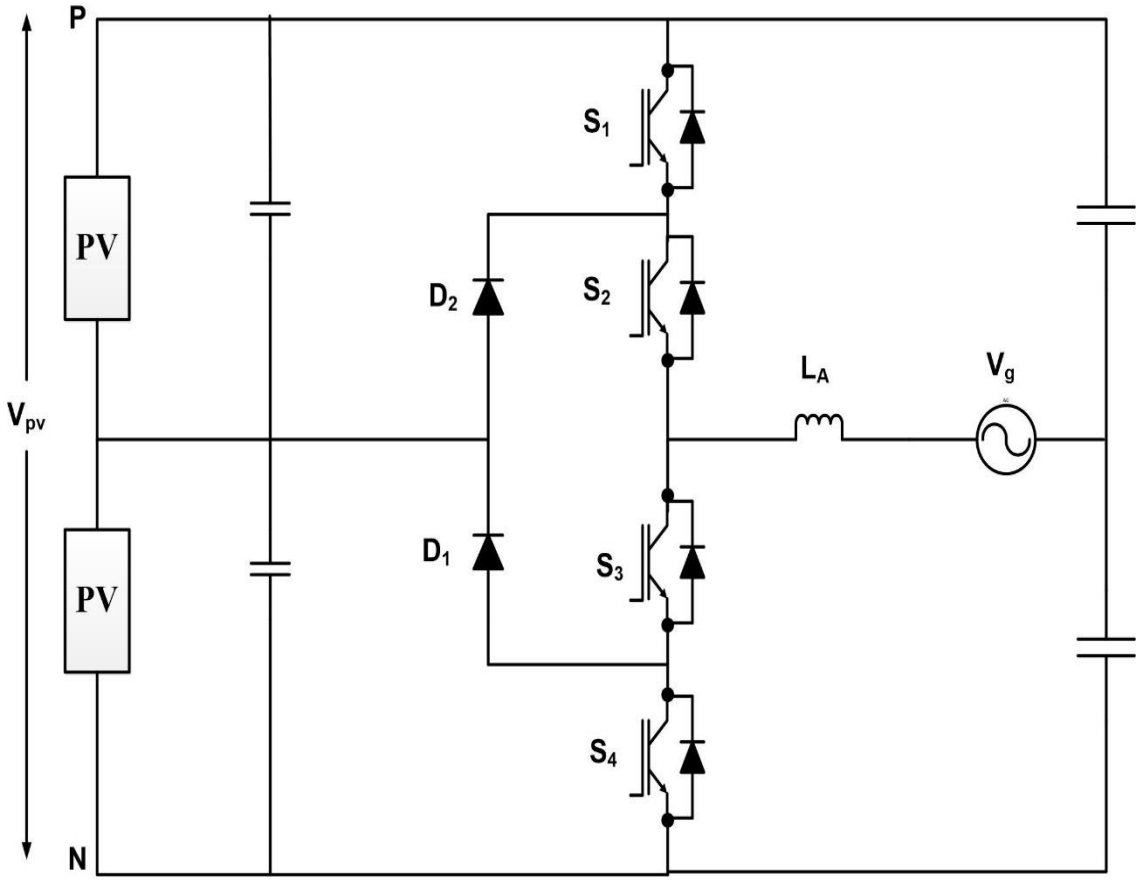

Fig. 2.15. NPC Topology

2.3.3.2. Flying Capacitor Topology [33]

In this topology the diodes which are clamped in the NPC topology are replaced by the capacitors. The capacitor acts as a floating element with respect to the DC link voltage. This topology has a drawback of the creation of imbalance voltages which may destroy the inverter.

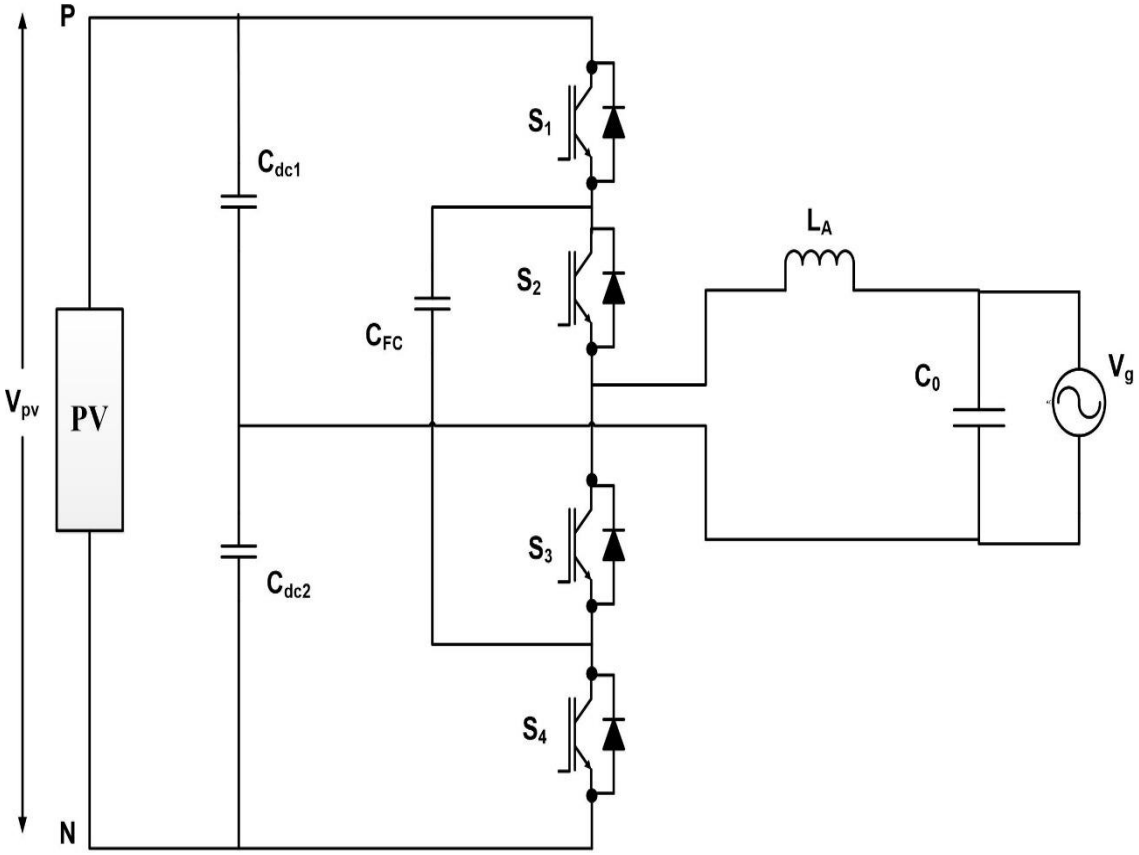

Fig. 2.16. Flying Capacitor Topology

2.4. CONCLUSION

In this chapter the basic components for a grid connected PV system has been discussed. Firstly different models for a PV cell are studied and modelling for single diode PV and double diode PV is carried on. The single diode models are further divided into ideal model, regular model and simplified model and it is concluded from the equations that the simplified model is most suited for the simulation purposes.

Secondly different MPPT algorithms are studied and conclusions are made on their advantages and disadvantages. Incremental Conductance MPPT is algorithm is chosen in this work for the control scheme to extract the maximum power from the two subarrays under varied conditions of irradiance and temperature.

In the end various single phase transformerless inverter topologies has been classified and discussed. The operation, advantages, disadvantages, number of switches used are discussed and has been compared in Table 2.2. After studying the various inverter topologies a modified version of the HERIC topology has been used in the inverter in Chapter 3 for connecting two PV subarrays to the inverter.

	Transformerless topologies	**Input Capacitor**	**Switches**	**Diodes**	**Leakage Current**
Zero-state decouple transformerless topologies	H5 topology	1	5	0	Medium
	HERIC topology	1	6	0	Very Low
Zero-state mid-point clamped transformerless topologies	H6 topology	2	6	2	Low
	oH5 topology	2	6	0	Medium
Solidity clamped transformerless topologies	NPC three-level VSI	2	4	2	Low
	Flying capacitor topology	3	4	0	Low

Table 2.2 Comparative Analysis on Transformerless Inverter Topologies

CHAPTER 3

OPERATING PRINCIPLE OF THE SCHEME

In this chapter the detailed discussion of the studies inverter topology is carried on. The operation of the inverter with various operating modes has been studied. Mathematical modelling for the small state model of the inverter is also derived.

3.1. GENERAL

The transformerless grid-tied inverters have the advantages of low cost, less bulky and less weight. But since there is no transformer large number of modules are needed to be connected in series. Due to this under varied operating conditions of the PV modules the power yield from each module is reduced substantially [34]-[36]. The topologies with NPC structure as discussed in Chapter 2 have a disadvantage since they require double the PV voltage [32][37].

To make the complexity easy the desired number of PV modules are connected in series which is chosen by the input voltage required. The main aim of the scheme studied in this thesis is to divide the PV subarrays into 2 modules which is then exposed to varying atmospheric conditions and extract maximum power from the two subarrays according to the operating conditions [38]. The advantages of using two PV modules means that the power yield would not decrease with the change in the operating conditions. The two series subarrays strategies is described in [38]-[40].

3.2. SCHEME STUDIED

In this thesis the studied inverter topology is similar to the HERIC topology describe in [29]. It is a combination of two H-bridge inverters combined with their AC bypasses. The scheme requires half the DC link voltage than the scheme proposed in [39]. Due to this the serially connected modules are half in number and hence the power yield is better. The proposed scheme has an advantage a low leakage current also. This increases the overall efficiency of the scheme.

The inverter topology is given in Fig. 3.1 below. The first half bridge is designed using switches S_1, D_1 and S_3, D_3 and its AC bypass consists of the switches S_5, D_5 and S_6, D_6. Similarly to second half bridge is designed using switches S_2, D_2 and S4, D_4 while its AC bypass consists of the switches S_7, D_7 and S_8, D_8. L_1, C_{o1}, L_2, and C_{o2} forms the output filters of the bridge 1 and bridge 2 respectively. PV_1 and PV_2 are the two PV subarrays with C_{f1} and C_{f2} as their input side filter capacitors. C_{pv0}, C_{pv1}, C_{pv2} are the parasitic ground capacitors. The leakage currents flows through these capacitors. These parasitic capacitors has been taken into consideration for the simulation part but neglected for the analysis part [32].

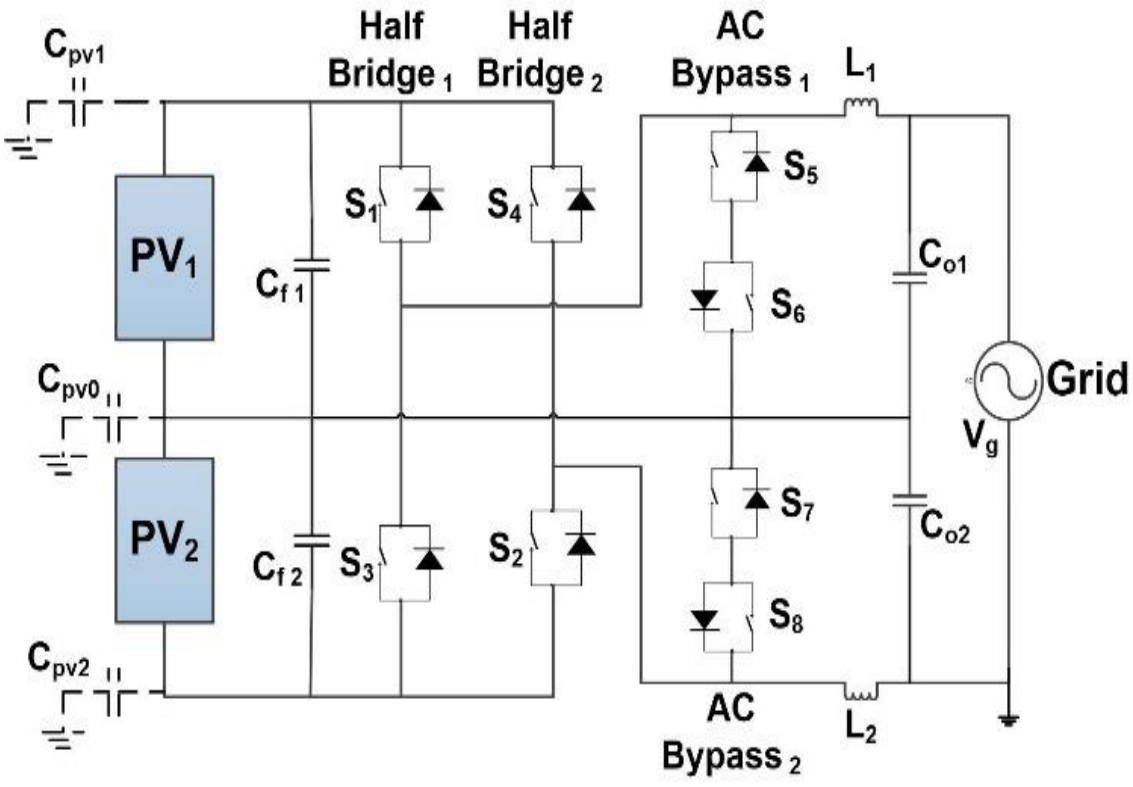

Fig. 3.1. Power Circuit for the Proposed Topology

In the positive half cycle, S_1 and S_2 switches operate with a sinusoidally varying duty cycle d_1 and d_2 and the AC bypass switches S_6 and S_8 are always on. Similarly in the negative half cycle the S_3 and S_4 switches are varied with sinusoidal duty cycles d_3 and d_4 and the switches S_5 and S_7 are always kept on. This change in the sinusoidal duty cycle ensures that under the unity power factor condition the Ig (grid current) is in synchronism with Vg (grid voltage) [38].

The inverter topology can be regarded as a modified HERIC topology as discussed in Chapter 2. The general HERIC topology is made to operate with a single input DC voltage but in the inverter scheme studied two input DC sources as two PV panels are taken into consideration. The PV panels are made to throw their power on capacitors C_{o1} and C_{o2} according to the positive or negative half cycle. The switching states for the studied inverter is given in Table 3.1.

S_1	**S_2**	**S_3**	**S_4**	**S_5**	**S_6**	**S_7**	**S_8**	**Voltage at C_{o1}**	**Voltage at C_{o2}**
ON	ON	OFF	OFF	OFF	OFF	OFF	OFF	$+V_{PV1}$	$+V_{PV2}$
OFF	OFF	OFF	OFF	OFF	ON	OFF	ON	0	0
OFF	OFF	ON	ON	OFF	OFF	OFF	OFF	$-V_{PV2}$	$-V_{PV1}$
OFF	OFF	OFF	OFF	ON	OFF	ON	OFF	0	0

Table 3.1. Switching States of Inverter

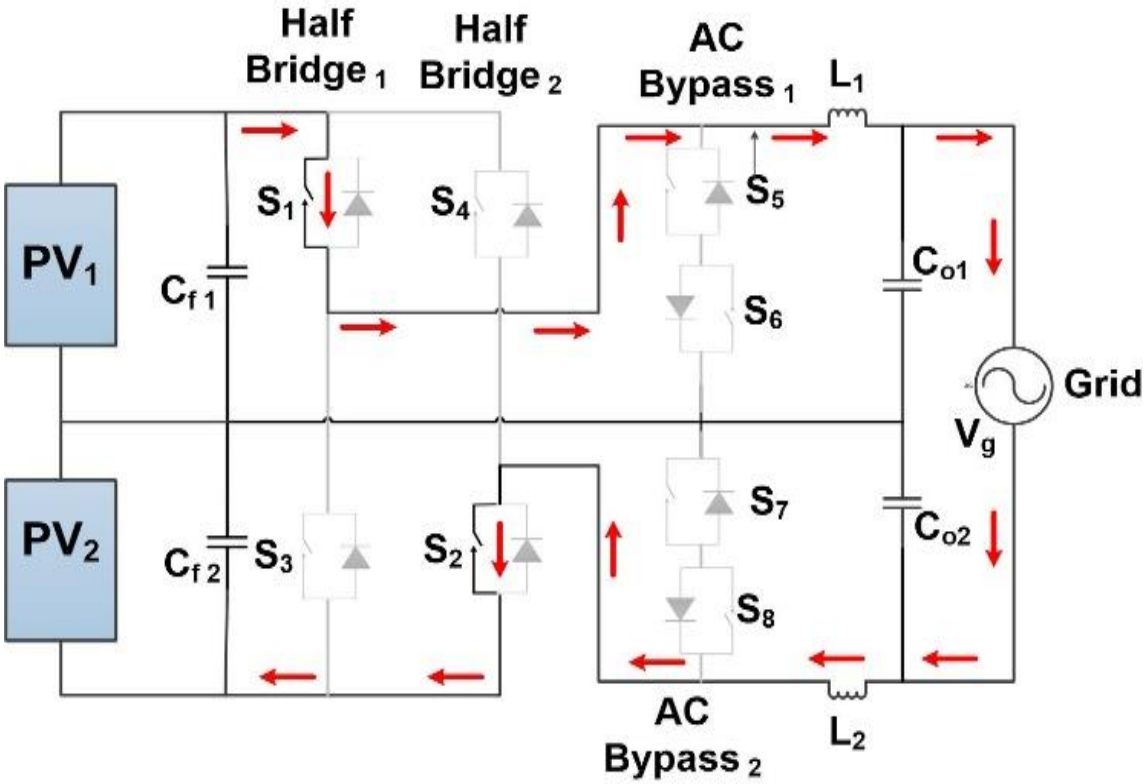

Fig. 3.2. Active Stage of Inverter in Positive Half Cycle

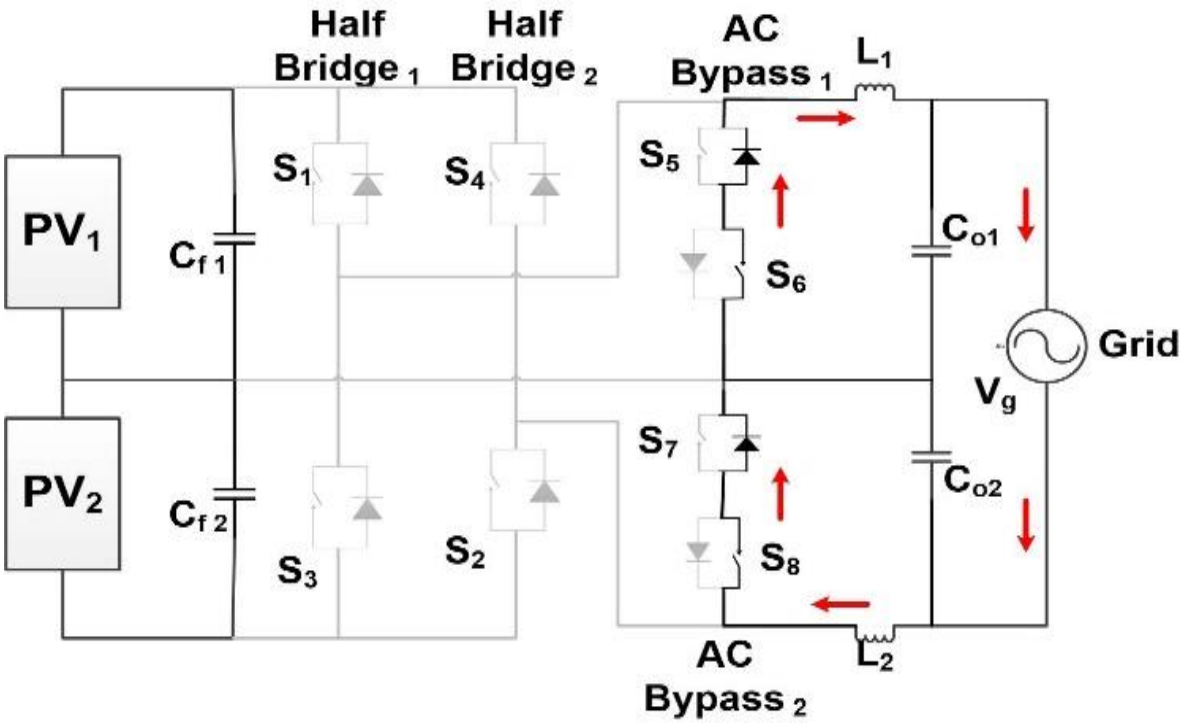

Fig. 3.3. Freewheeling Stage of Inverter in Positive Half Cycle

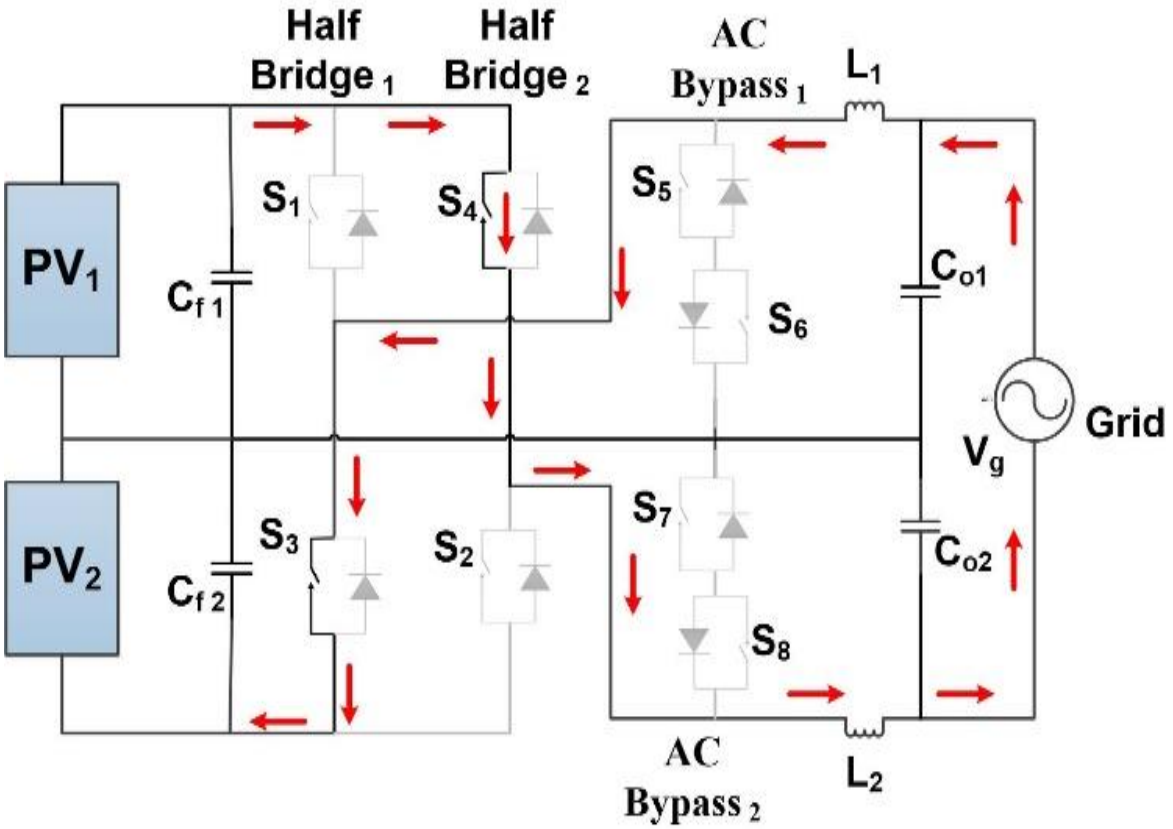

Fig. 3.4. Active Stage of Inverter in Negative Half Cycle

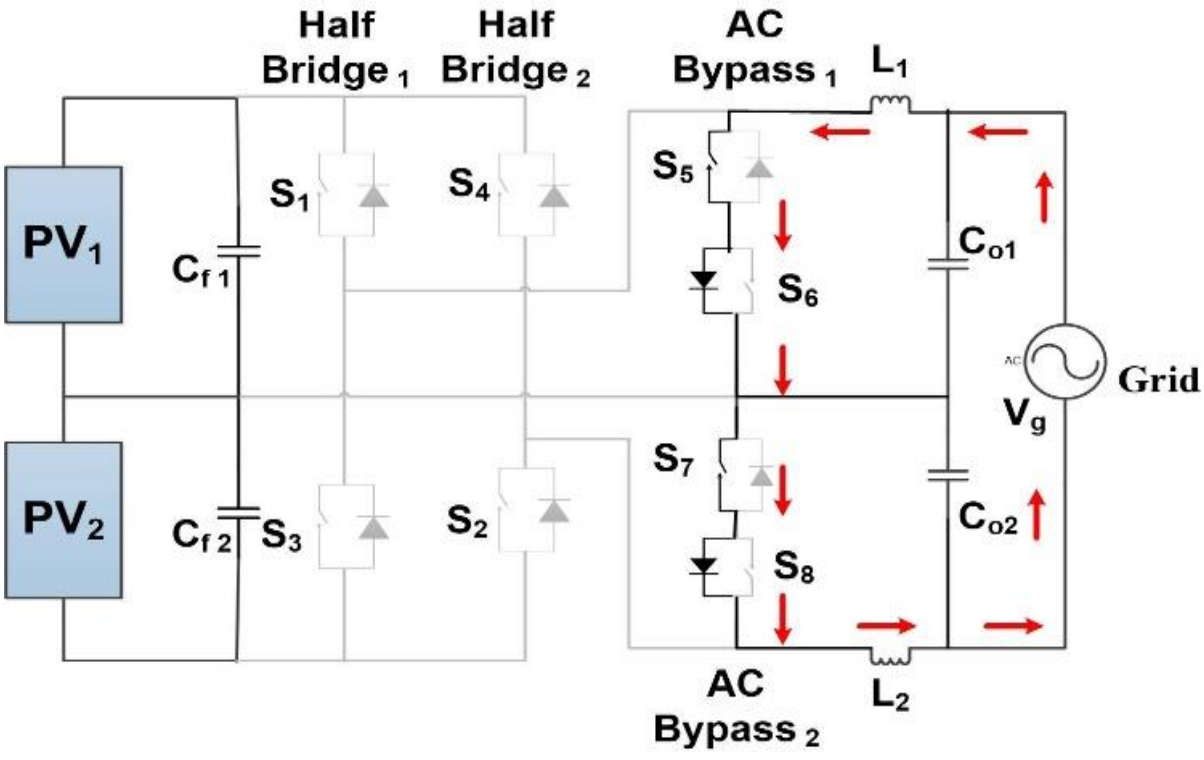

Fig. 3.5. Freewheeling Stage of Inverter in Negative Half Cycle

The analysis of the scheme can be simplified with Fig. 3 and Fig. 4. Since the PV subarrays are subjected to varying insolation level and temperature level the output power, output DC voltage and the current for both the subarrays would be different. P_{MPP1}, V_{MPP1} and I_{MPP1} are the maximum power, voltage and current for PV subarray 1 and P_{MPP2}, V_{MPP2} and I_{MPP2} is for the PV subarray 2. During the positive half cycle the power from PV_1 and PV_2 is given to C_{o1} and C_{o2} while in the negative half cycle the power from PV_1 and PV_2 are dumped at C_{o2}, C_{o1} [38].

During the positive half cycle,

$$P_{gco1} = P_{MPP1} \tag{3.1}$$

$$P_{gco2} = P_{MPP2} \tag{3.2}$$

During the negative half cycle,

$$P_{gco1} = P_{MPP2} \tag{3.3}$$

$$P_{gco2} = P_{MPP1} \tag{3.4}$$

Whereas the powers P_{gco1} and P_{gco2} are the average powers for the half cycle. The total average power P_g to the grid is given by

$$P_g = P_{MPP1} + P_{MPP2} \tag{3.5}$$

$$v_g = v_{co1} + v_{co2} \tag{3.6}$$

Where, v_g: instantaneous grid voltage,

v_{co1} and v_{co2}: voltages across the capacitors C_{o1} and C_{o2}.

The grid power P_g is given as

$$P_g = v_g i_g = (v_{co1} + v_{co2}) i_g \tag{3.7}$$

As inverter is made to operate under unity power factor. Hence,

$$I_g = \frac{P_g}{V_g} \tag{3.8}$$

where I_g and V_g are the rms current and voltage of the grid.

1. During Positive Half Cycle

$$P_g = \frac{1}{\pi}\int_0^{\pi} v_{co1} i_g d(wt) + \frac{1}{\pi}\int_0^{\pi} v_{co2} i_g d(wt) \quad (3.9)$$

$$= P_{gco1} + P_{gco2} \quad (3.10)$$

Hence

$$P_{gco1} = \frac{1}{\pi}\int_0^{\pi} V_{co1m} \sin(wt)\, I_{gm} \sin(wt) d(wt)$$

$$= \frac{V_{co1m} I_{gm}}{2} \quad (3.11)$$

$$P_{gco2} = \frac{1}{\pi}\int_0^{\pi} V_{co2m} \sin(wt)\, I_{gm} \sin(wt) d(wt)$$

$$= \frac{V_{co1m} I_{gm}}{2} \quad (3.12)$$

$$V_{co1m} = \frac{2P_{MPP1}}{I_{gm}} = \frac{\sqrt{2}P_{MPP1}}{I_g} = \frac{\sqrt{2}P_{MPP1}}{P_g / V_g} \quad (3.13)$$

$$V_{co2m} = \frac{2P_{MPP2}}{I_{gm}} = \frac{\sqrt{2}P_{MPP2}}{I_g} = \frac{\sqrt{2}P_{MPP2}}{P_g / V_g} \quad (3.14)$$

Using (3.5), (3.13) and (3.14)

$$V_{co1m} = \frac{\sqrt{2}V_g P_{mpp1}}{P_{MPP1} + P_{MPP2}} \quad (3.15)$$

$$V_{co2m} = \frac{\sqrt{2}V_g P_{mpp2}}{P_{MPP1} + P_{MPP2}} \quad (3.16)$$

2. During Negative Half Cycle

$$P_{gco1} = \frac{1}{\pi}\int_0^{\pi} V_{co2m} \sin(wt)\, I_{gm} \sin(wt) d(wt)$$

$$= \frac{V_{co2m} I_{gm}}{2} \quad (3.17)$$

$$P_{gco2} = \frac{1}{\pi}\int_0^{\pi} V_{co1m}\sin(wt)\, I_{gm}\sin(wt)d(wt)$$

$$= \frac{V_{co1m}I_{gm}}{2} \tag{3.18}$$

$$V_{co1m} = \frac{2P_{MPP2}}{I_{gm}} = \frac{\sqrt{2}P_{MPP2}}{I_g} = \frac{\sqrt{2}P_{MPP2}}{P_g/V_g} \tag{3.19}$$

$$V_{co2m} = \frac{2P_{MPP1}}{I_{gm}} = \frac{\sqrt{2}P_{MPP1}}{I_g} = \frac{\sqrt{2}P_{MPP1}}{P_g/V_g} \tag{3.20}$$

Using (3.5), (3.19) and (3.20)

$$V_{co1m} = \frac{\sqrt{2}V_g P_{mpp2}}{P_{MPP1}+P_{MPP2}} \tag{3.21}$$

$$V_{co2m} = \frac{\sqrt{2}V_g P_{mpp1}}{P_{MPP1}+P_{MPP2}} \tag{3.22}$$

From the equations (3.15), (3.16), (3.21) and (3.22) it is proved the the magnitudes of the voltages V_{co1m} and V_{co2m} are dependent on the PV power.

The duty ratios for positive half cycle varies sinusoidal which is given by (3.23) while the duty ratios for the negative half cycle is given by (3.24).

$$d_{1m} = \frac{V_{co1m}}{V_{MPP1}} \quad \text{and} \quad d_{2m} = \frac{V_{co2m}}{V_{MPP2}} \tag{3.23}$$

$$d_{3m} = \frac{V_{co1m}}{V_{MPP2}} \text{ and } d_{4m} = \frac{V_{co2m}}{V_{MPP1}} \tag{3.24}$$

Since the half bridge inverters with their bypass are connected in series, it is assumed that the current going through the filter capacitors L_1 and L_2 are equal i.e. $i_{L1}=i_{L2}=i_g$. Here we are neglecting the currents passing through C_{o1} and C_{o2}.

3.3. MATHEMATICAL MODELLING

The mathematical model of the scheme can be described by the equivalent circuits shown in Fig. 3.6 and Fig. 3.7 The figure describes the operating of the active and the freewheeling state for positive half cycle. L_1 and L_2 are considered as the filter inductors and R_{L1} and R_{L2} are the parasitic resistances for both the filter inductors respectively. The series resistances for the filter capacitors are neglected which would not affect the result to a great level but it would reduce the complexity. Since our main aim is to control the injected grid current i_g. This current is dependent on the current through both the filter inductors L_1 and L_2 and the voltages across the filter capacitors C_{o1} and C_{o2}. Therefore these four variables are considered as the state variables [38].

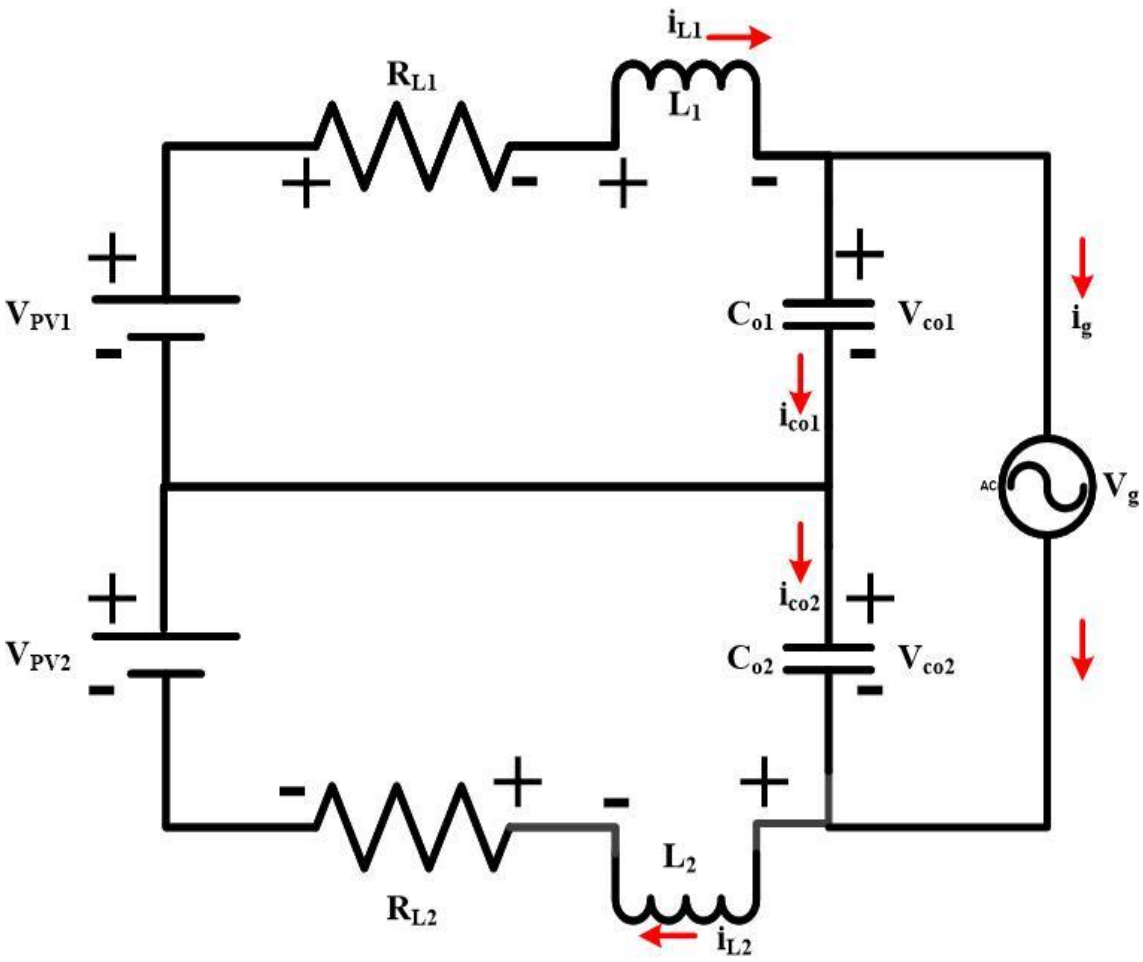

Fig. 3.6. Equivalent Circuit of the system for Positive Half Cycle in Active State.

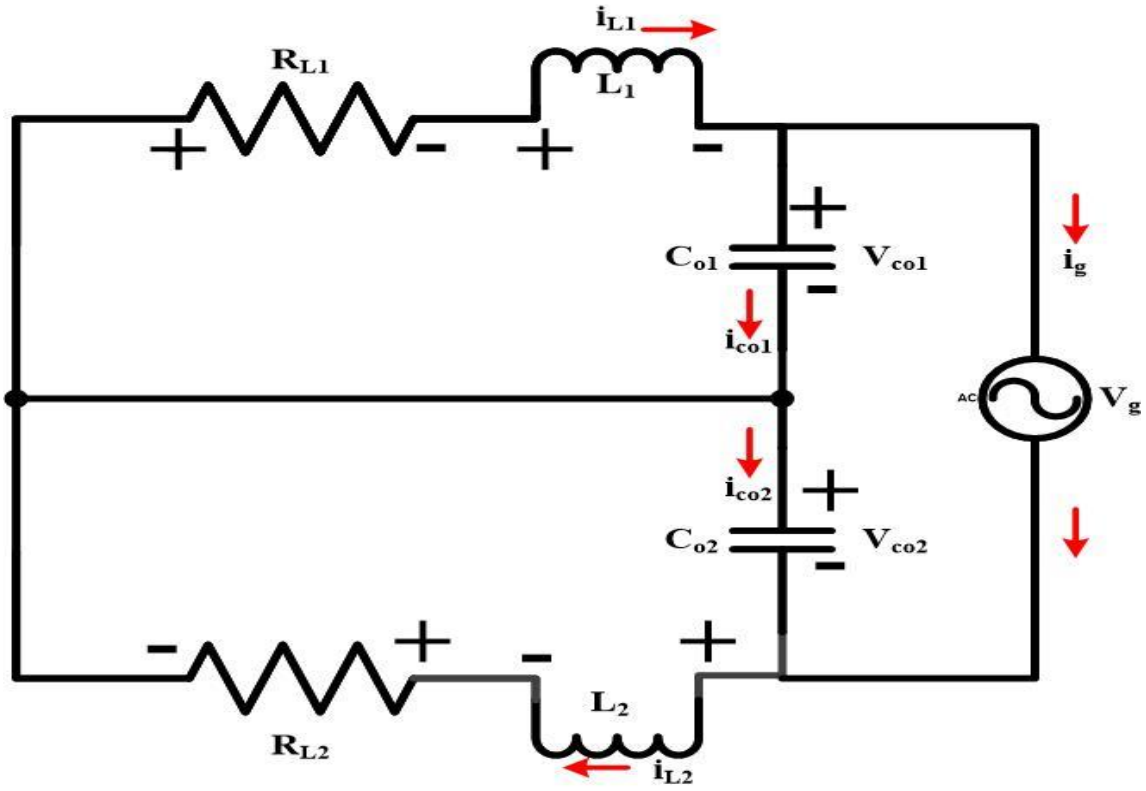

Fig. 3.7. Equivalent Circuit of the system in Positive Half Cycle in Freewheeling State.

The state equations can be derived from both the H-bridge circuits with their respective AC bypasses. For the first half bridge the state equations can be described as

$$\frac{d}{dt}\begin{bmatrix} i_{L1}(t) \\ v_{co1}(t) \end{bmatrix} = \begin{bmatrix} -\frac{R_{L1}}{L_1} & -\frac{1}{L_1} \\ \frac{1}{C_{o1}} & 0 \end{bmatrix}\begin{bmatrix} i_{L1}(t) \\ v_{co1}(t) \end{bmatrix} + \begin{bmatrix} \frac{1}{L_1} & 0 \\ 0 & -\frac{1}{Z_g C_{o1}} \end{bmatrix}\begin{bmatrix} v_{pv1}(t) \\ v_g(t) \end{bmatrix} \tag{3.25}$$

$$\frac{d}{dt}\begin{bmatrix} i_{L1}(t) \\ v_{co1}(t) \end{bmatrix} = \begin{bmatrix} -\frac{R_{L1}}{L_1} & -\frac{1}{L_1} \\ \frac{1}{C_{o1}} & 0 \end{bmatrix}\begin{bmatrix} i_{L1}(t) \\ v_{co1}(t) \end{bmatrix} + \begin{bmatrix} 0 & 0 \\ 0 & -\frac{1}{Z_g C_{o1}} \end{bmatrix}\begin{bmatrix} v_{pv1}(t) \\ v_g(t) \end{bmatrix} \tag{3.26}$$

For the second H-bridge the state equations can be derived as

$$\frac{d}{dt}\begin{bmatrix} i_{L2}(t) \\ v_{co2}(t) \end{bmatrix} = \begin{bmatrix} -\frac{R_{L2}}{L_2} & -\frac{1}{L_2} \\ \frac{1}{C_{o2}} & 0 \end{bmatrix}\begin{bmatrix} i_{L2}(t) \\ v_{co2}(t) \end{bmatrix} + \begin{bmatrix} \frac{1}{L_2} & 0 \\ 0 & -\frac{1}{Z_g C_{o2}} \end{bmatrix}\begin{bmatrix} v_{pv2}(t) \\ v_g(t) \end{bmatrix} \tag{3.27}$$

$$\frac{d}{dt}\begin{bmatrix} i_{L2}(t) \\ v_{co2}(t) \end{bmatrix} = \begin{bmatrix} -\frac{R_{L2}}{L_2} & -\frac{1}{L_2} \\ \frac{1}{C_{o2}} & 0 \end{bmatrix}\begin{bmatrix} i_{L2}(t) \\ v_{co2}(t) \end{bmatrix} + \begin{bmatrix} 0 & 0 \\ 0 & -\frac{1}{Z_g C_{o2}} \end{bmatrix}\begin{bmatrix} v_{pv2}(t) \\ v_g(t) \end{bmatrix} \quad (3.28)$$

here $i_g(t) = Z_g\, v_g(t)$ where Z_g is the grid impedance for the short circuit condition. The state space average technique is applied the equations are written in s-domain. The transfer function with the duty cycle and the filter currents for the positive half cycle is given below

$$\frac{i_{L1}(s)}{d(s)} = \frac{C_{o1} V_{pv1} s}{L_1 C_{o1} s^2 + R_{L1} C_{o1} s + 1} \quad (3.29)$$

$$\frac{i_{L2}(s)}{d(s)} = \frac{C_{o2} V_{pv2} s}{L_2 C_{o2} s^2 + R_{L2} C_{o2} s + 1} \quad (3.30)$$

$$\frac{v_{co1}(s)}{d(s)} = \frac{V_{pv1}}{L_1 C_{o1} s^2 + R_{L1} C_{o1} s + 1} \quad (3.31)$$

$$\frac{v_{co2}(s)}{d(s)} = \frac{V_{pv2}}{L_2 C_{o2} s^2 + R_{L2} C_{o2} s + 1} \quad (3.32)$$

Similarly the above equations can be derived for the negative half cycle given as:

$$\frac{i_{L1}(s)}{d(s)} = \frac{C_{o1} V_{pv2} s}{L_1 C_{o1} s^2 + R_{L1} C_{o1} s + 1} \quad (3.33)$$

$$\frac{i_{L2}(s)}{d(s)} = \frac{C_{o2} V_{pv1} s}{L_2 C_{o2} s^2 + R_{L2} C_{o2} s + 1} \quad (3.34)$$

$$\frac{v_{co1}(s)}{d(s)} = \frac{V_{pv2}}{L_1 C_{o1} s^2 + R_{L1} C_{o1} s + 1} \quad (3.35)$$

$$\frac{v_{co2}(s)}{d(s)} = \frac{V_{pv1}}{L_2 C_{o2} s^2 + R_{L2} C_{o2} s + 1} \quad (3.36)$$

3.4. SELECTION OF PASSIVE ELEMENTS

3.4.1. Selection of Input Filter Capacitance (C_{f1} and C_{f2})

The following formula is used to obtain the input capacitance value [34],

$$C_{f1} = C_{f2} = \frac{P_{mpp1}}{2\omega\Delta V_{ripple} V_{min}^2} = \frac{P_{mpp2}}{2\omega\Delta V_{ripple} V_{min}^2} \quad (3.37)$$

where, ω = angular grid frequency

Min. Input Voltage:V_{min} = 190V,

ΔV_{ripple} = 1.9 V.

3.4.2. Selection of filter inductances L_1 and L_2

The formula for the filter inductances is given as [34],

$$L_1 = L_2 = \frac{V_{com}\Delta I_{factor}}{f_{sw}\Delta I_L} \quad (3.38)$$

where V_{com} = 190V, ΔI_{factor} = 0.12 which is the maximum ripple factor, f_{sw}=20 KHz which is the switching frequency and ripple in inductor current, ΔI_l=0.25A.

3.4.3. Selection of Filter Capacitance C_{o1} and C_{o2}

The filter capacitance values are obtained from [34],

$$C_{o1} = C_{o2} = \frac{1}{4\pi^2 f_c^2 (L_1 \text{ or } L_2)} \quad (3.39)$$

where f_c=1 KHz is the cut off frequency.

3.4. CONCLUSION

In this chapter, the inverter topology and the general scheme of the system has been studied. The switching states of the inverter is defined for positive and negative half cycles and the freewheeling state. The operation of the scheme is also been studied with mathematical equations. The small signal model has been derived. The values of the passive elements such as input filter capacitance, output filter inductance and output filter capacitance has been obtained using [34] and the actual values of these elements are defined in chapter 4 (refer table 4.1).

CHAPTER 4

PROPORTIONAL INTEGRAL CONTROLLER

In this chapter control strategy for the proposed inverter has been discussed. Here a conventional Proportional Integral Controller (PIC) has been taken into consideration. The results for the PI control strategy has also been discussed.

4.1. PROPORTIONAL INTEGRAL CONTROLLER (PIC)

The simulated control strategy is shown in Fig. 4.1, Fig. 4.2 and Fig. 4.3. Here the two subarrays are able to monitor the MPP with the help of Incremental Conductance MPPT Algorithm. The obtained voltages at MPP are then compared with the actual PV voltages to generate an error which is then processed to PI controllers.

A PLL is used to track the frequency of the voltage v_g. This grid frequency is imposed on a unity amplitude sinusoidal function to generate the signal X. The signal X is basically a sinusoidal signal with unity amplitude and the frequency of this signal is equal to the grid frequency and changes with the change in grid frequency.

The output of the PI controllers and signal X are multiplied to generate the reference currents I_{ref1} and I_{ref2}. These reference currents are used to control the filter currents I_{L1} and I_{L2} which eventually controls the grid current I_g.

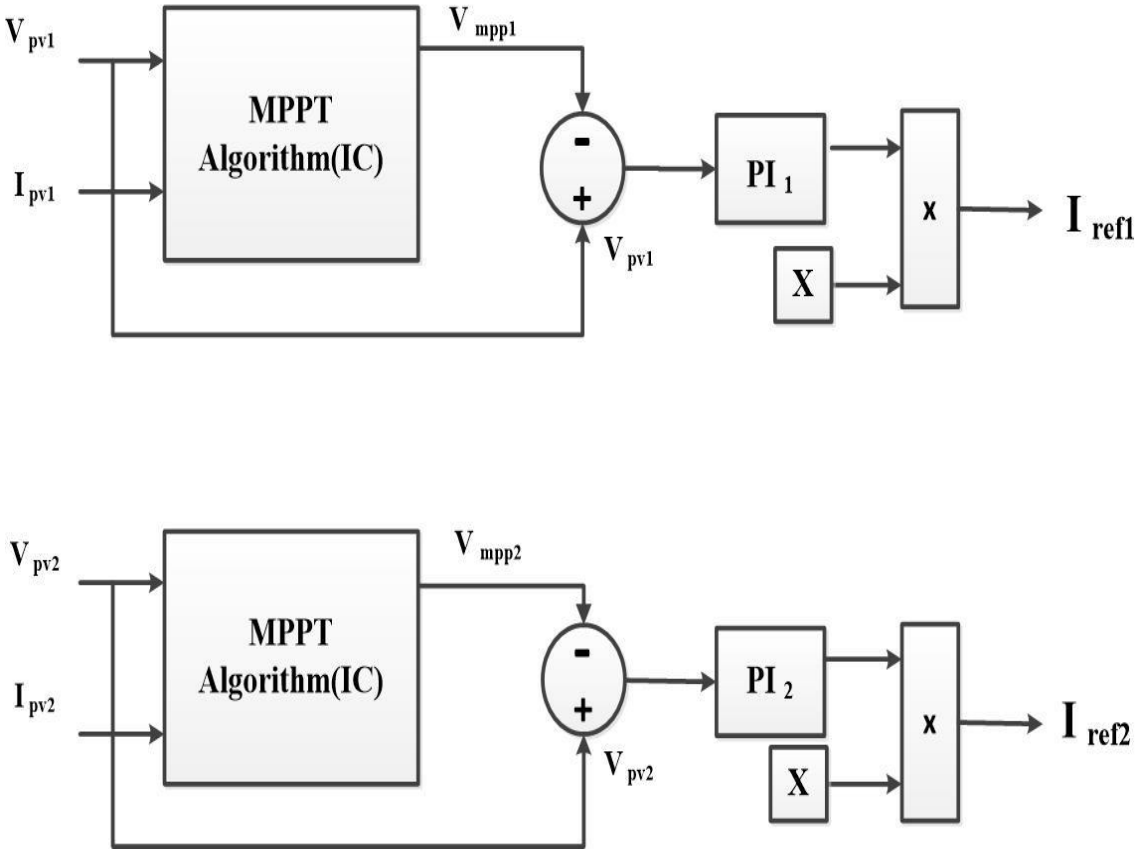

Fig. 4.1. Reference Current Generation

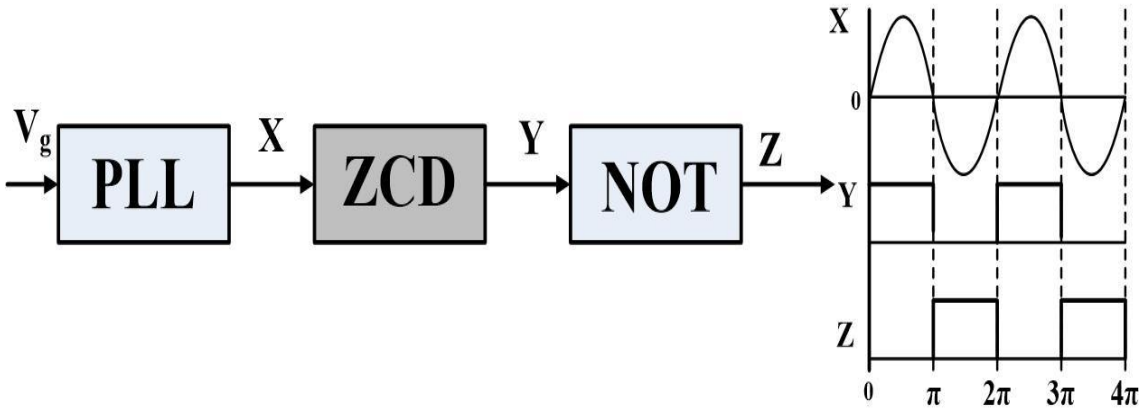

Fig. 4.2. Grid voltage synchronism with PLL

During the positive half cycle as shown in Fig. 3.2 the module PV_1 controls the current in inductor L_1 through switch S_1 and module PV_2 controls the current in inductor L_2 through switch S_2. Hence it is shown in Fig. 7 when X > 0 (i.e. positive half cycle) I_{ref1} is compared with i_{L1} and I_{ref2} is compared with i_{L2}.

During negative half cycle as shown in Fig. 3.4 module PV_1 controls the current in inductor L_2 through the switch S_4 and module PV_2 controls the current in inductor L_1 through switch S_3. Hence it is shown in Fig. 7 when X<0 (i.e. negative half cycle) I_{ref2} is compared with i_{L1} and I_{ref1} is compared with current i_{L2}.

The errors generated with the above comparisons are then given to two separate PI controllers to generate the sinusoidal varying duty ratios for the switches S_1-S_4.

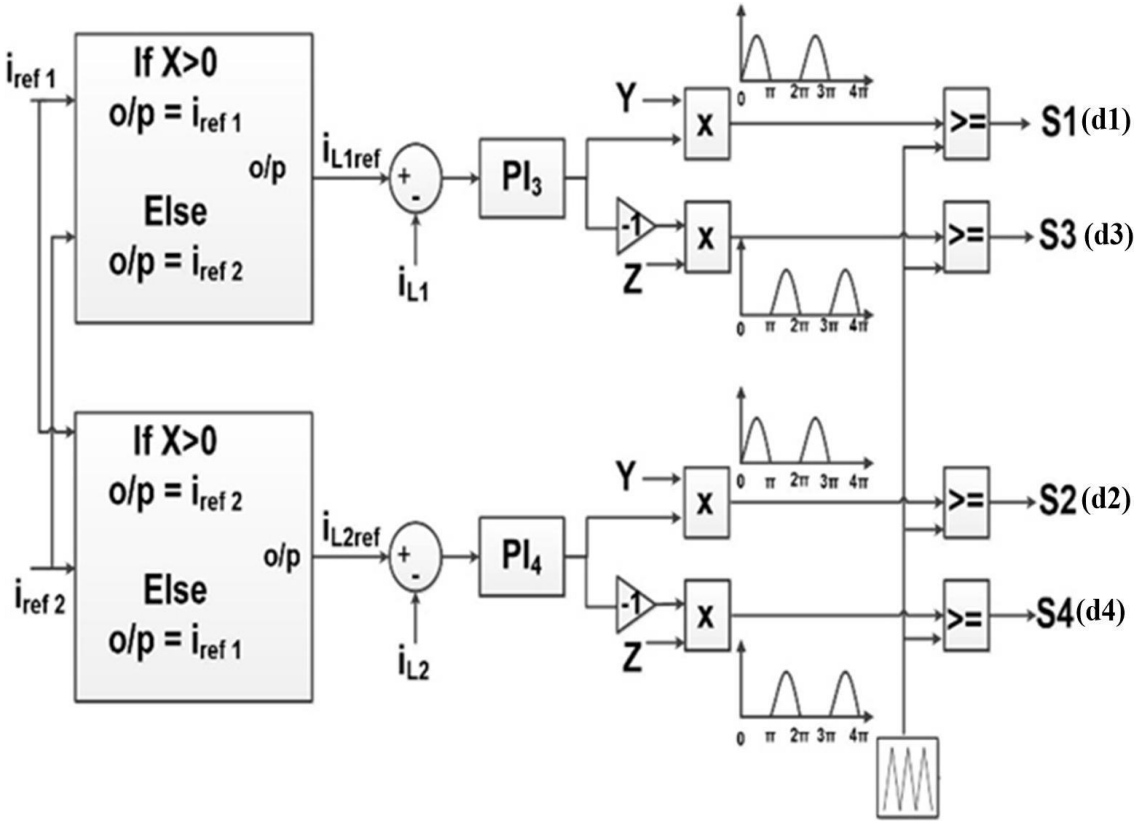

Fig. 4.3. Duty ratio generation for the switches

The criteria for the selection of K_p and K_i for the PI controller can be derived from the small signal model equations described in the previous chapter. The equations (3.29) and (3.30) are shown below

$$\frac{i_{L1}(s)}{d(s)} = \frac{C_{o1}V_{pv1}s}{L_1C_{o1}s^2 + R_{L1}C_{o1}s + 1} \tag{3.29}$$

$$\frac{i_{L2}(s)}{d(s)} = \frac{C_{o2}V_{pv2}s}{L_2C_{o2}s^2 + R_{L2}C_{o2}s + 1} \tag{3.30}$$

In the above equations the variation of the duty ratios with respect to the changes in inductor currents i_{L1} and i_{L2} have been derived. These inductor currents are the outputs of HB_1 and HB_2 respectively.

Here K_i for the PIC is kept constant at 100 and K_p is varied from 0.005 to 5. The frequency response for the above block diagram is plotted. The equation (3.29) and (3.30) are similar in the frequency sense hence we can use one of the above two equations. In this particular study equation (3.29) is taken into consideration.

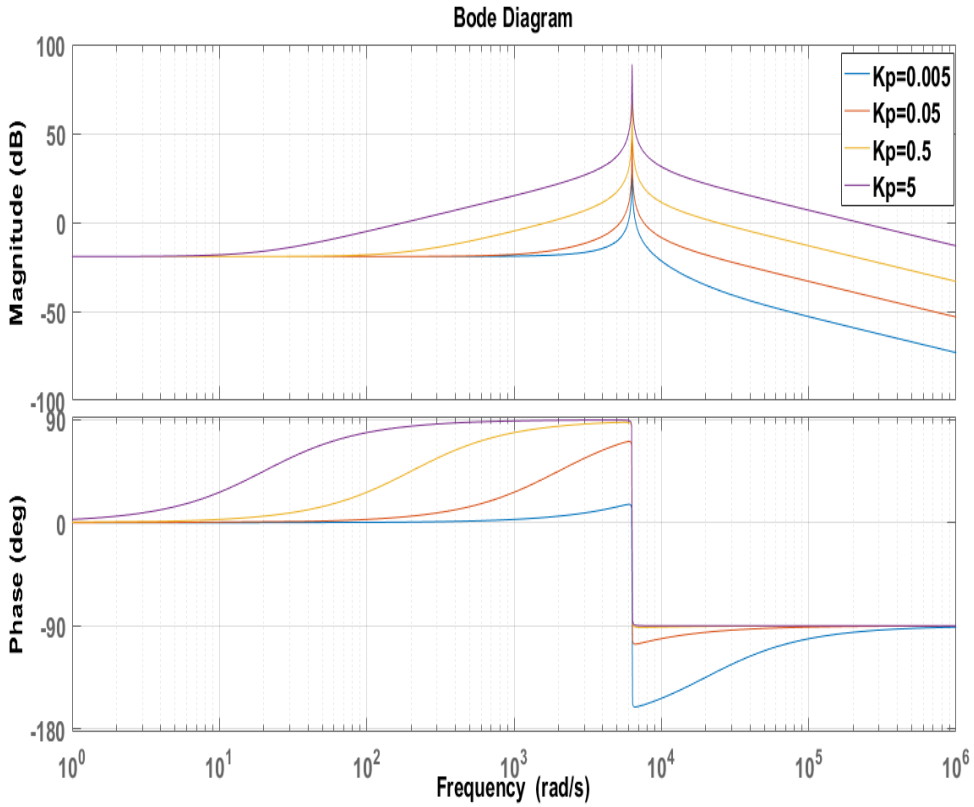

Fig. 4.5. Frequency Response with K_i = 100 and varying K_p.

It can be concluded from the above frequency plot that if the proportional gain is decreased the phase margin of the system also decreases which leads to instability. If the proportional gain is increase the phase margin also increases very small. Hence the value of K_p is selected as 0.5 since after increasing the proportional gain above this value the THD% of the grid current also increases.

4.2. SIMULATION AND RESULTS

The simulation for the grid tied inverter with two serially connected PV arrays which are both exposed to different atmospheric conditions has been simulated in MATLAB Simulink platform. The simulation has been run for 8s and the variation in the insolation and temperature has been provided in the Table I. The system parameters selection has been given in Table II. Results have been compared for DC voltages, currents and powers for both the PV panels separately. Both the PV panels are able to tract their MPP under varied atmospheric conditions.

Parameter	**Value**
Single Phase Grid Voltage (V_g)	230 V, 50 Hz
V_{oc}^a and V_{mpp} of subarrays	270 V and 217 V
I_{sc}^c and I_{mpp} of subarrays	3.58 A and 3.22 A
P_{mpp1} and P_{mpp2} at STC	780 W
Total Power	1.5 kW Approx
L_1 and L_2	5 mH
C_{o1} and C_{o2}	5 μF
C_{f1} and C_{f2}	3300 μF
Deployed MPPT Methodology	Incremental Conductance

Table 4.1. System Parameters

Time (s)	**0-1**	**1-2**	**2-3**	**3-4**	**4-6**	**6-8**
PV1 Insolation, kW/m^2	0.7	0.8	0.9	1	1	1
PV2 Insolation, kW/m^2	0.9	0.9	0.9	0.9	0.9	0.9

Temperature in PV_1, ^0C	25	25	25	25	30	35
Temperature in PV_2, ^0C	25	25	25	25	25	25

Table 4.2. Variation of Insolation and Temperature with time.

The simulation has been carried out in MATLAB-Simulink where the parameters for different parts of the system has been given in Table 4.1. The total power rating of the system is taken as around 1.5 kW with the maximum power of 780 W for each of the PV module. The grid voltage has been taken as 230 V with 50 Hz frequency.

Incremental Conductance MPPT algorithm is employed since it has the advantages of simple, robustness, fast response and it also does not oscillate around the power point as in other MPPT algorithms.

The results for the input side parameters for the PV modules has been shown in Fig. 4.6. Separate results has been taken for each PV module with V_{MPP1} and V_{MPP2} as the maximum voltage extracted from the PV modules PV_1 and PV_2 and similarly maximum currents I_{MPP1} and I_{MPP2} and maximum power P_{MPP1} and P_{MPP2} which has been extracted from both the PV panels respectively.

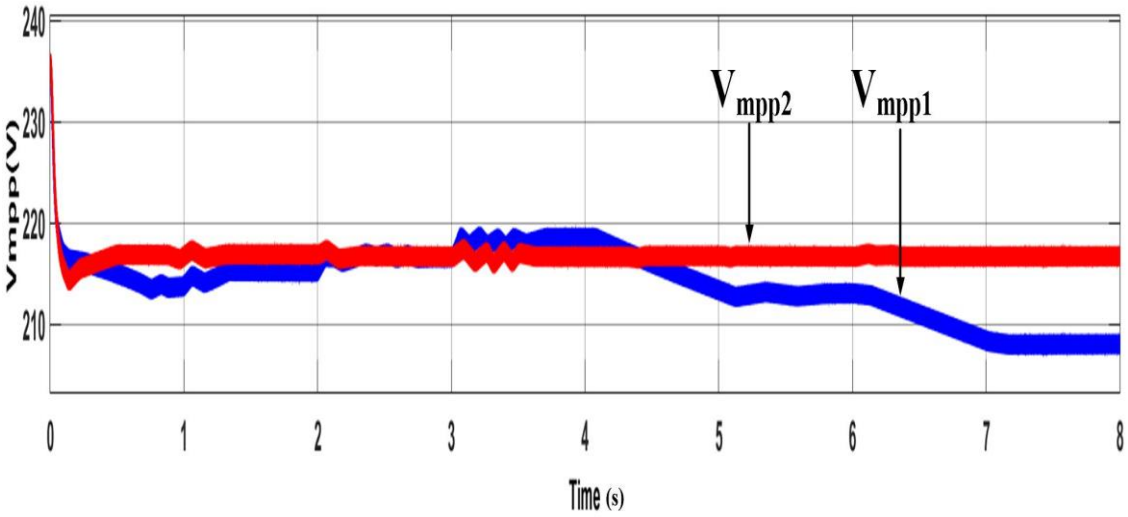

Fig. 4.6. Maximum Voltage Extracted from PV_1 and PV_2 : PI Controller

In Fig. 4.6 in the variation in voltage for the two PV panels are in accordance with the variation in irradiance and temperature as depicted in Table 4.2. For PV_1 there has been an increase in irradiance from t = 0 to t = 3 with constant temperature with steps of 1s. Therefore the V_{MPP1} is increasing in this time interval. After t = 4s the irradiance is kept constant and the temperature is increasing and hence the voltage is decreasing in accordance with the output characteristics of the PV cell. For PV_2 the irradiance and temperature is kept constant for the entire simulated time and therefore the voltage and the PV terminal is constant.

Similarly the variation of PV maximum PV currents and the power extracted from the modules has been shown in Fig. 4.7 and Fig. 4.8.

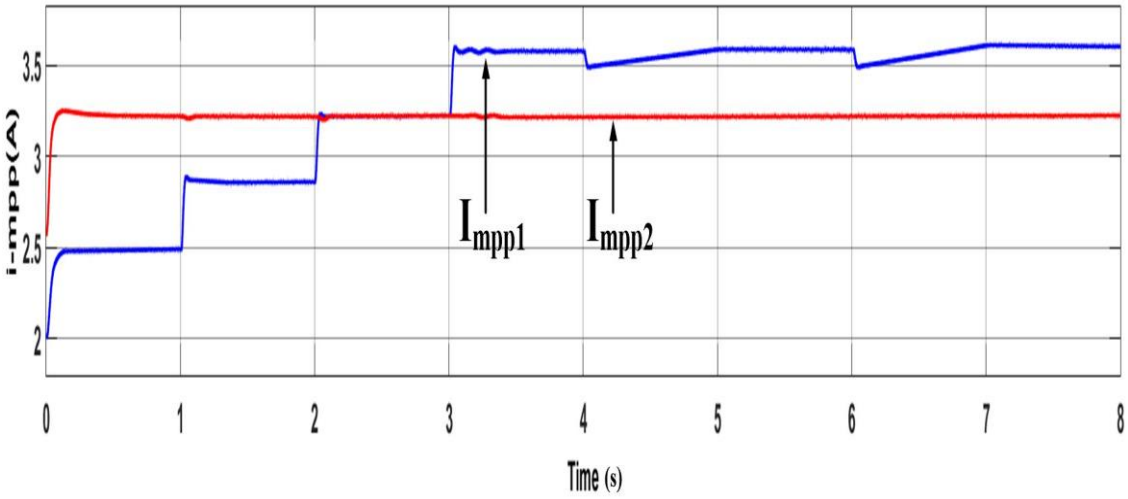

Fig. 4.7. Maximum Current Extracted from PV_1 and PV_2.

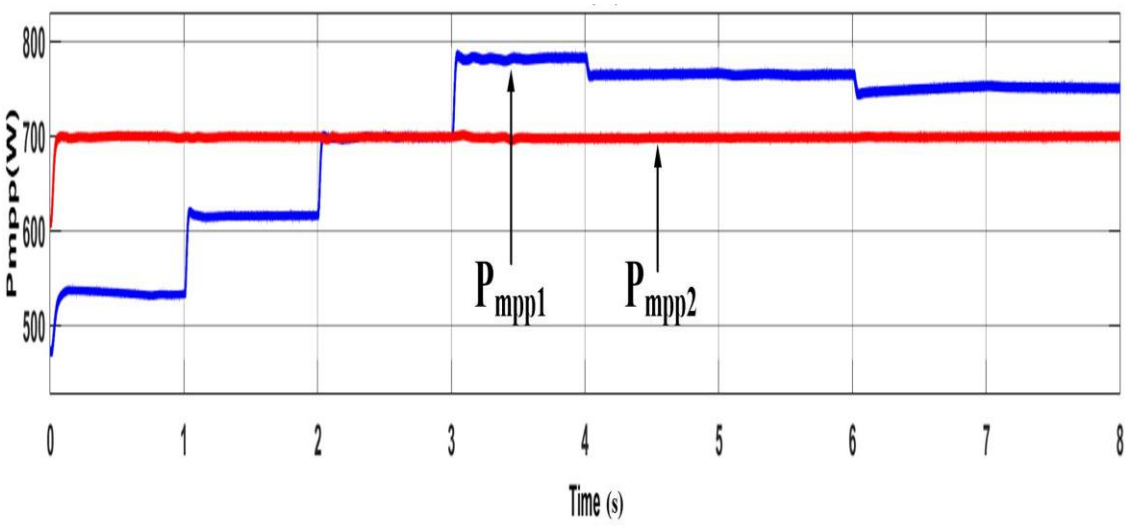

Fig. 4.8. Maximum Power Extracted from PV_1 and PV_2

The output parameters for the inverter are the grid current i_g and voltage across the filter capacitors C_{o1} and C_{o2}. The variation in i_g is shown in Fig. 4.9 for the entire simulated time of 8s. The variations in grid current with changing irradiance in depicted in Fig. 4.9 and it is concluded that as the irradiance increases the grid current increases.

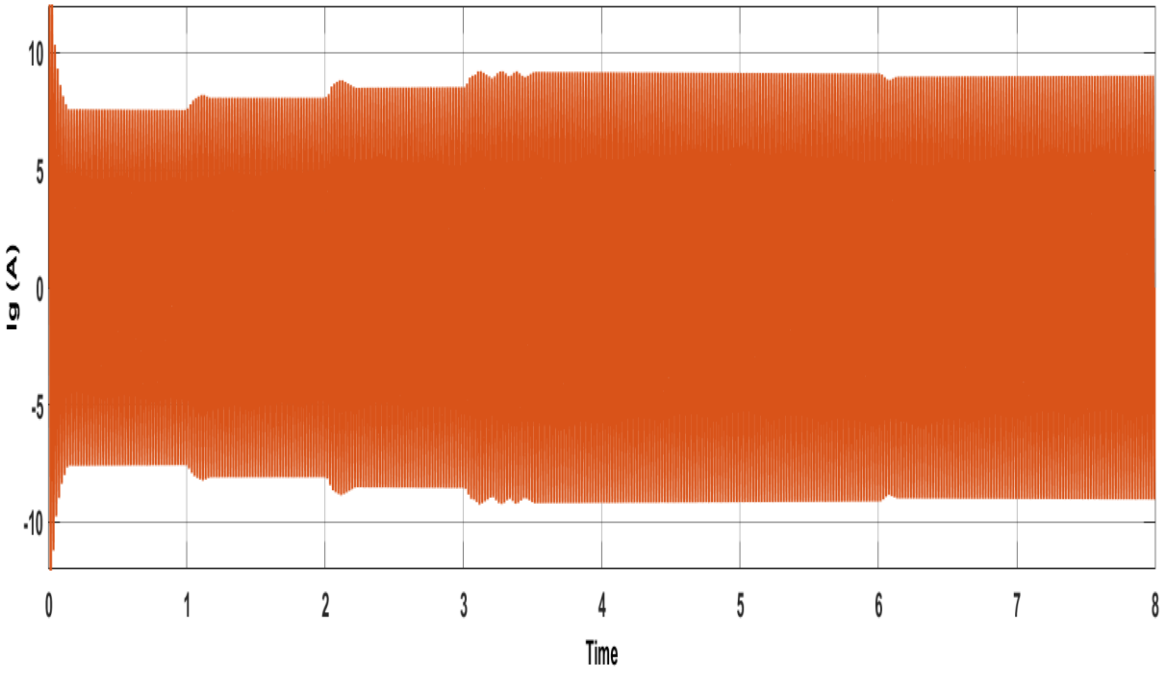

Fig. 4.9. Variation in Grid Current (i_g).

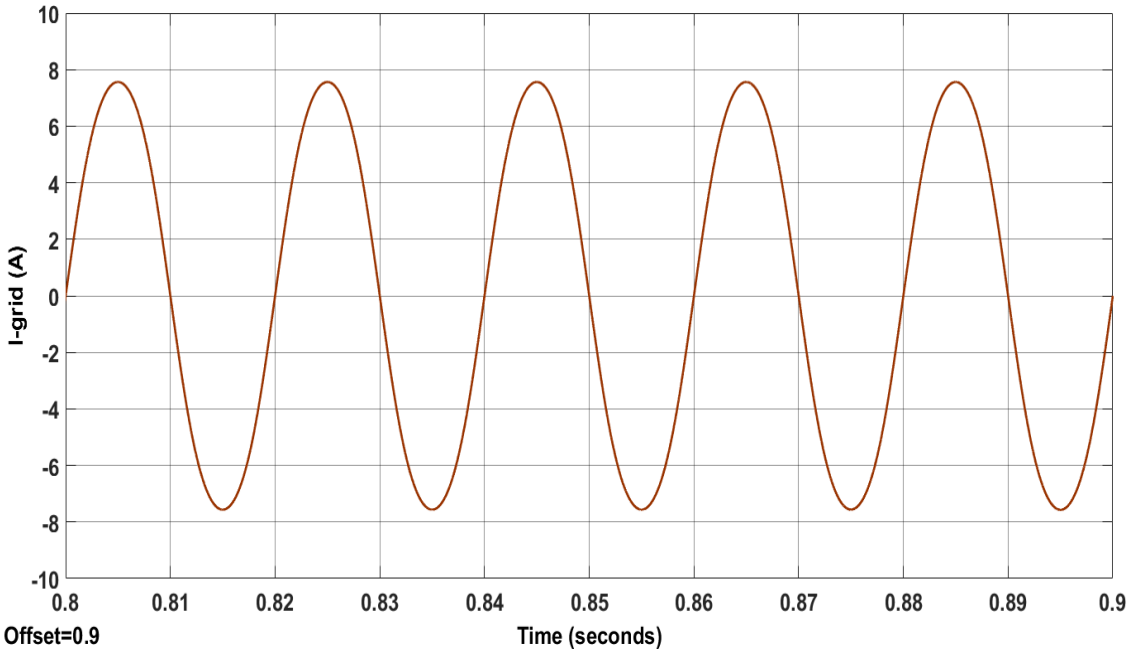

Fig. 4.10. Magnified Version of Grid Current i_g (A) for 5 cycles from t=0.8s to t=0.9s

In Fig. 4.11 the magnified version of the grid current with grid voltage v_g is shown. The grid voltage has been reduced with a gain of 1/30 so that the phase difference between grid current and voltage is clearly visible. It is concluded from Fig. 4.11 that the grid voltage and currents are in phase with each other and hence the inverter is working with unity power factor as described in Chapter 3 equation (3.8). The magnified version of the voltage and current is taken for 5 cycles in time interval t= 0.8s to t= 0.9s.

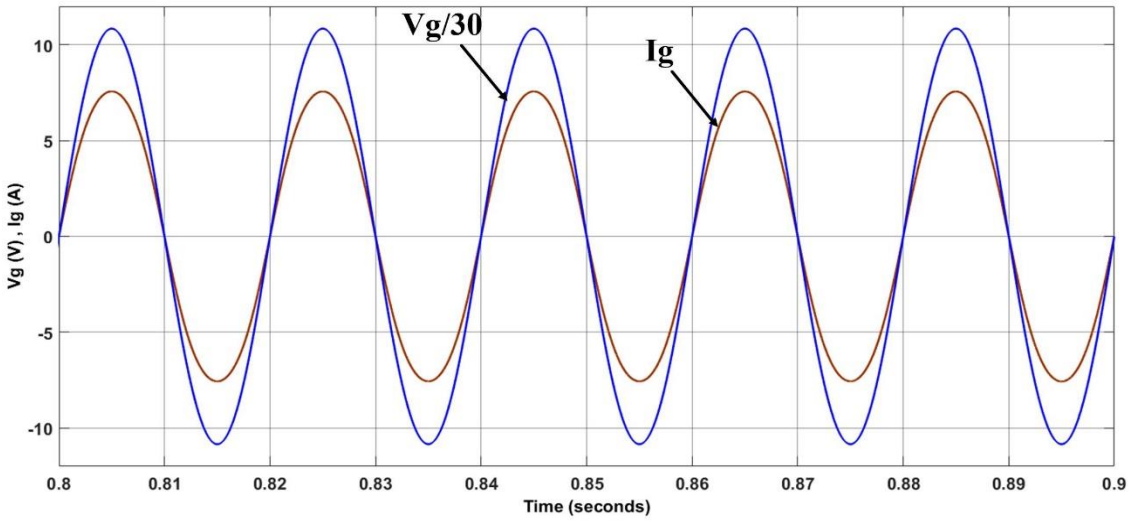

Fig. 4.11. Magnified Version of Grid Current i_g (A) and voltage v_g (V): t = 0.8s to t = 0.9s.

The variation in voltages across the filter capacitors V_{co1} and V_{co2} is shown in Fig. 4.11 and the magnified version of the same is shown in Fig. 4.12. From Fig. 4.12 it is concluded for the positive and negative half cycles the amplitude of the voltages varies and it is in accordance with equation (3.15), (3.16), (3.21) and (3.22) from Chapter 3. The sum of both the voltages is always equal to the grid voltage.

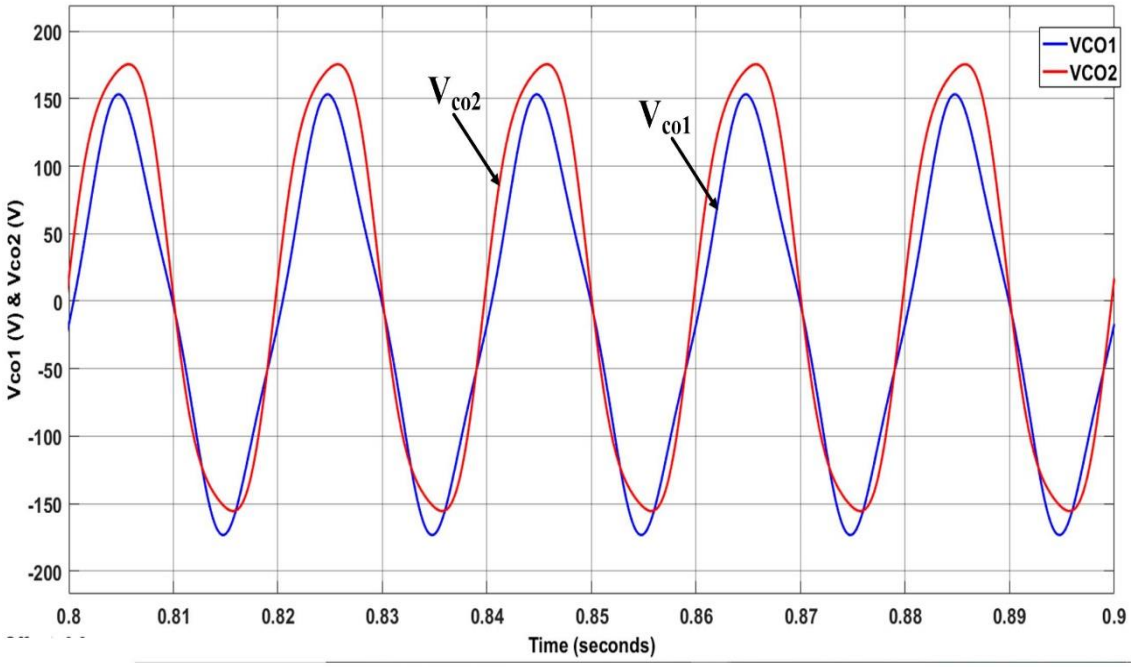

Fig. 4.12. Variation in V_{co1} and V_{co2} for t= 0.8s to t= 0.9s.

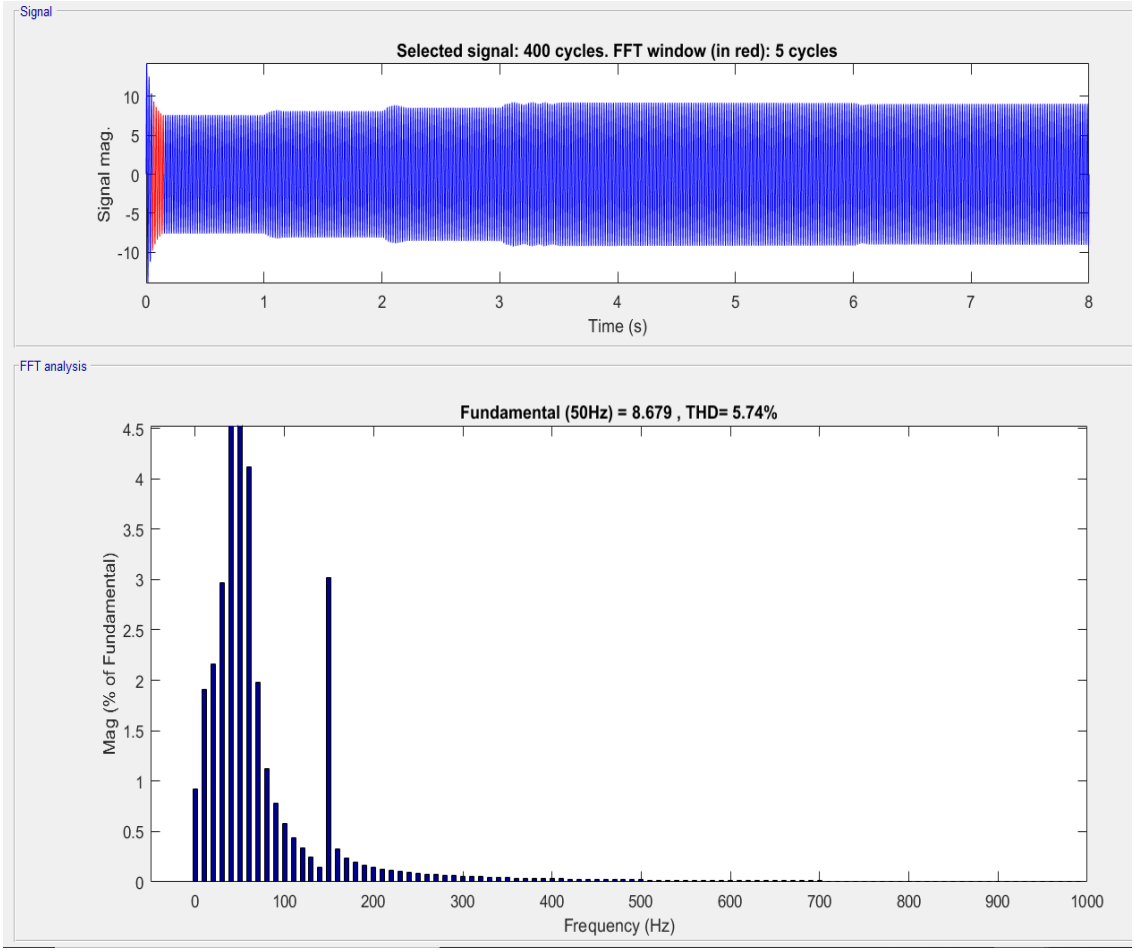

Fig. 4.13 : THD% for injected grid current i_g taken for 5 cycles = 5.74%

4.3. CONCLUSION

In this chapter, the synchronization of the inverter topology as discussed in chapter 3 is done with a single phase grid. A decoupled control strategy for positive and negative half cycles is discussed. A conventional PI controller is used in the control scheme and to evaluate the correct tuning of the PI controller frequency response of the duty cycle as input and inverter current as output is derived for different values of K_i and K_p. It can be concluded from the frequency plot that keeping K_i constant as 100 if the proportional gain is decreased the phase margin of the system also decreases which leads to instability. If the proportional gain is increase the phase margin also increases very small. Hence the value of K_p is selected as 0.5 since after increasing the proportional gain above this value the THD% of the grid current also increases.

The results have been obtained for the performance of the inverter where the input side DC quantities of voltage, current and power is plotted for both the PV subarrays separately with varying conditions of irradiance and temperature for both the subarrays and it is concluded that the maximum power has been extracted from both the PV subarrays in accordance with the operating conditions of irradiance and temperature. The output side quantities of the inverter has also been plotted with grid current and THD% of the grid current. The grid voltage and current are plotted together and it is concluded that the grid voltage is in phase with the grid current hence validating the operation of the inverter with unity power factor as discussed in chapter 3.

CHAPTER 5

FUZZY LOGIC CONTROLLER

In this chapter control strategy for the proposed inverter has been discussed. Here a Fuzzy Logic Controller (FLC) has been taken into consideration. The results for the FLC control strategy has been discussed.

5.1. GENERAL

Fuzzy Logic Controller is one of the simplest controller for inverter control in grid connected PV systems. It does not require the mathematical modelling of the control system and can be derived with the help of if-else conditions. The fuzzy controllers are better than the conventional PI controllers in terms of response, settling time and output THD% [41].

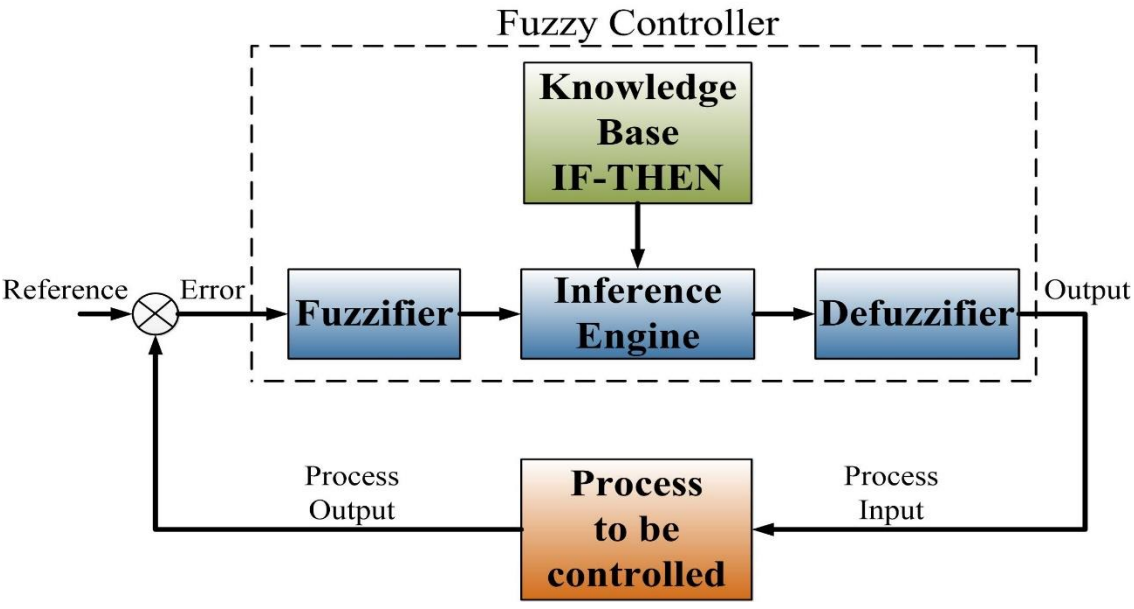

Fig. 5.1. Fuzzy Logic Architecture

Since the nature of the inverter is non-linear the fuzzy controller is highly suitable for the control of the inverter [42]. The general architecture of the FLC is shown in Fig. 5.1. The three main components of this fuzzy architecture are fuzzifier system, ruling system and defuzzifier system. The other units of this architecture are the input error signal to the controller unit and the unit to be controlled. In our case it is the inverter duty cycle for the switches [43].

5.1.1. Fuzzy Interference

The fuzzy unit produce the output according to the if-else rules based on the system [44]. The fuzzy output system converts all the sets from the output to produce crisp outputs [45]. The Mamdani interference method which has been used in this work is more popular than the other methods such as Sugeno style.

5.1.2. Fuzzification

Before processing the input data in the system degree to which the physical values (crisps) of each input belong in the appropriate fuzzy sets should be determined. Thus the input signals are taken into the membership function which decides the degree for the input [46].

5.1.3. Defuzzification

This is the last step of the inference system. This process involves the production of crisp output values with fuzzy sets. The centroid method is one of the method used to convert fuzzy sets to crisp sets and it has been used in this work also. This method identifies the centre of gravity point from the fuzzy set in the given interval of k=1 to n [45][46].

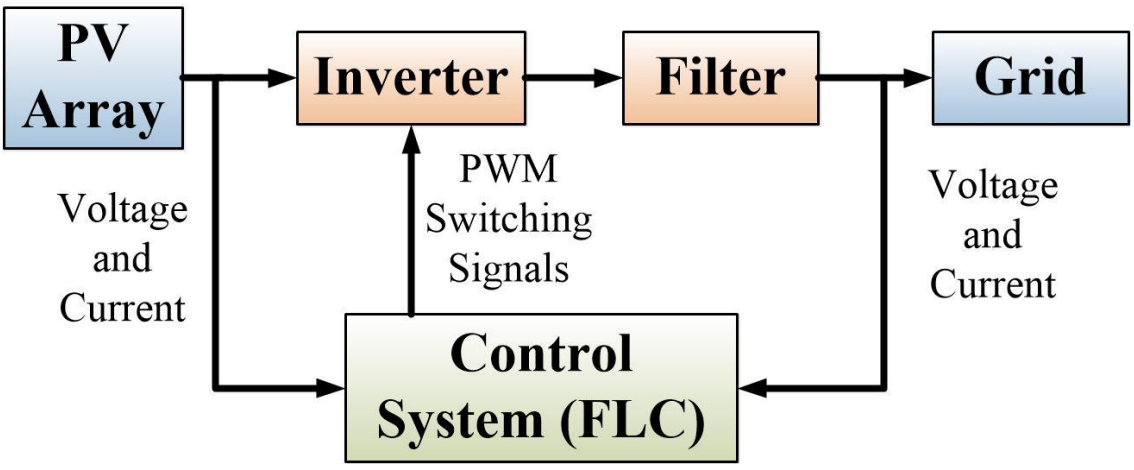

Fig. 5.2. General Grid Tied PV Control System using Fuzzy Logic Controller

5.2. FUZZY LOGIC CONTROLLER (FLC)

The simulated control strategy is depicted in Fig. 5.1 for the fuzzy logic controller. Here the error signal is taken from the difference of the signals i_{Lref} and i_L for both the PV panels. The derivative is also taken and the error signal and its derivative is taken as the input to the fuzzy logic controller. The fuzzy controller consists of the fuzzification, the rule based system and deffuzification. The rule based system is the main brain of the system which contains the membership functions.

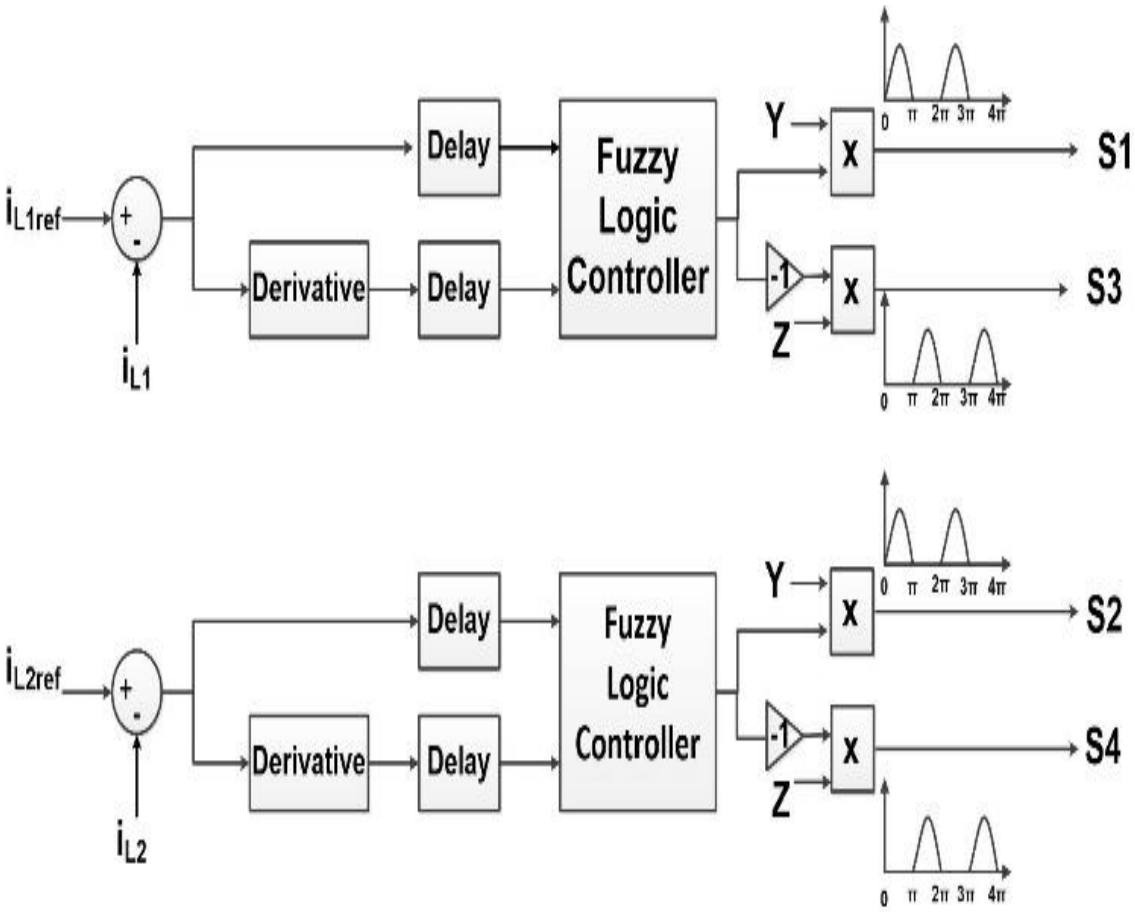

Fig. 5.3. Fuzzy Logic Control Scheme

For the fuzzy logic controller error and its derivative are taken as the two inputs. The two inputs have 3 Gaussian Membership functions. The membership functions have a standard deviation of 0.4247. The linguistic variables are “Negative” [N], “Positive [P] and “Zero” [Z]. The mean value for these functions are -1,1 and 0 respectively.

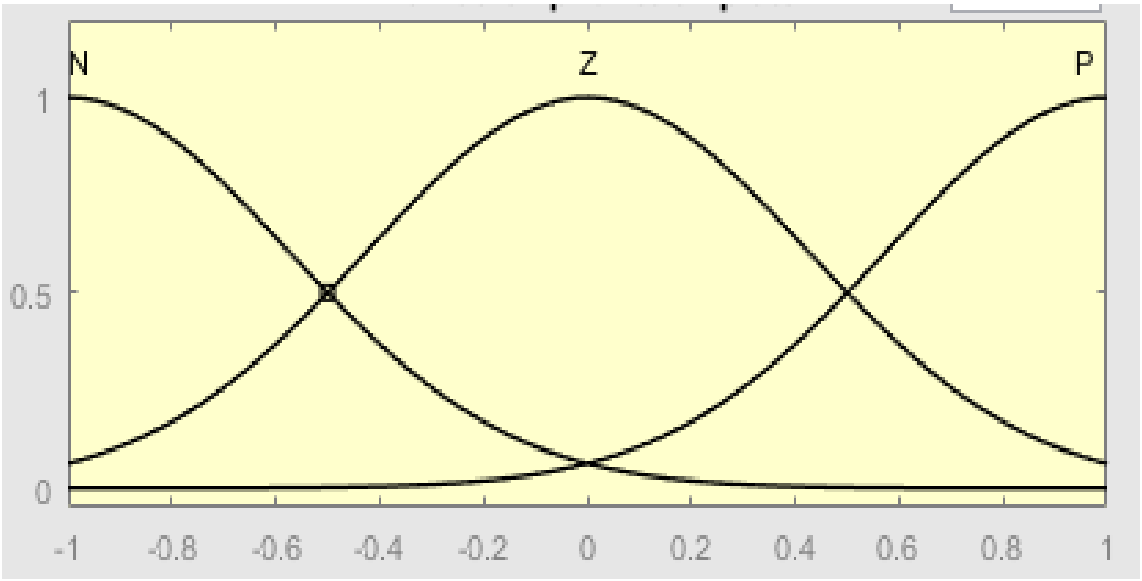

Fig. 5.4. Membership functions for the input variables of the Fuzzy Logic Controller.

The control action is then defuzzified with a five membership functions to a unity value as shown in Fig. 5.4. The output variables are taken as “Big Negative” [BN], “Negative” [N], “Zero” [Z], “Positive” [P] and “Big Positive” [BP].

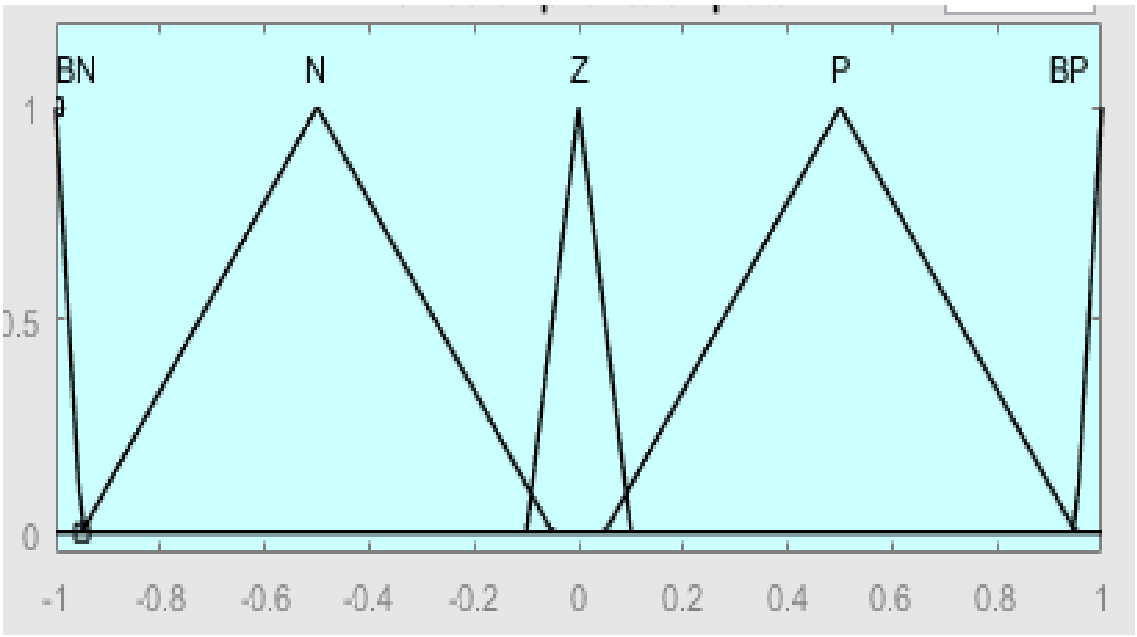

Fig. 5.5. Output Variables for the Fuzzy System after applying the rules

The rules are established on the basis of information about the system and its operation according to variations of error and change in error inputs to obtain fast transient response. The rule bases of the fuzzy logic for output variables are seen in Table 5.1.

E / dE/dt	N	Z	P
N	BN	BN	BN
Z	P	Z	N
P	BP	BP	BP

Table 5.1. Rules for Fuzzy System

5.3. SIMULATION AND RESULTS

63

.0The results for the FLC is obtained using the same parameters as from Table 4.1 and Table 4.2 from Chapter 4. The input side parameters are plotted with maximum voltage, current and power of the two PV panels.

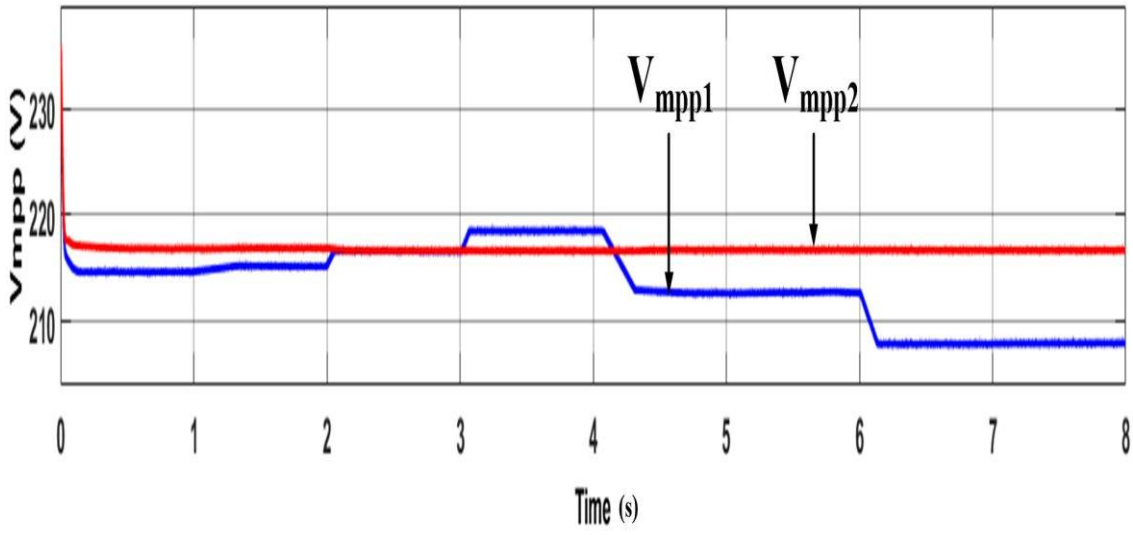

Fig. 5.6. Maximum Voltage (V) Extracted from PV_1 and PV_2 : FLC

It is concluded from Fig. 5.4 that the FLC is able to control the voltage better than the PI controller. For PV_1 in the time interval t=4sec to t=6sec the settling time for FLC in 0.3sec whereas it is higher for PI controller. Similar observation can be made for time t=6 sec to t=8 sec since it takes only 0.1 sec to settle which is much lower than the PI controller.

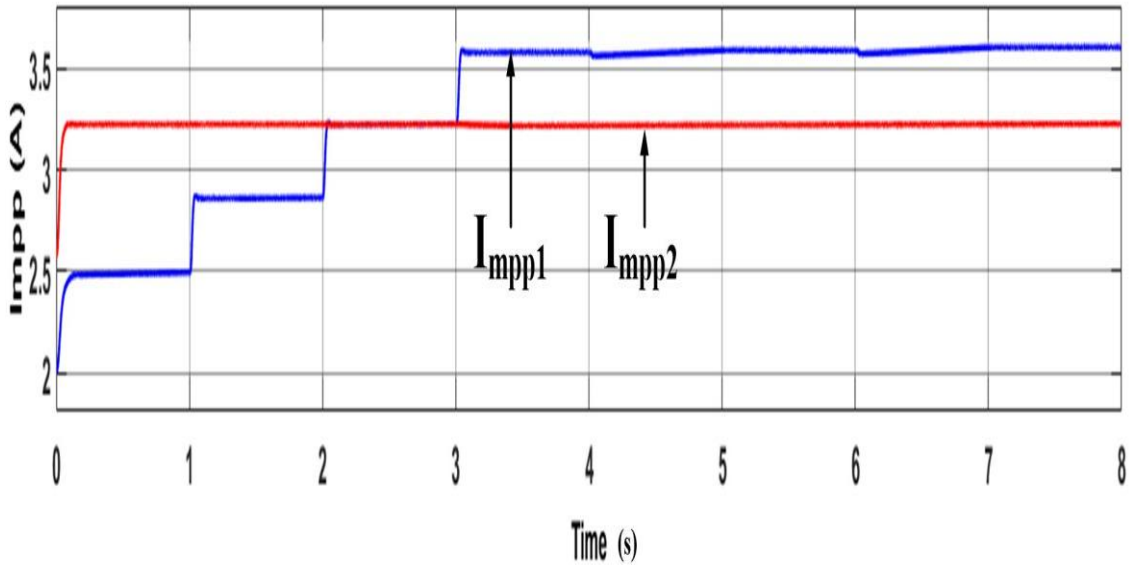

Fig. 5.7. Maximum Current (A) Extracted from PV_1 and PV_2.

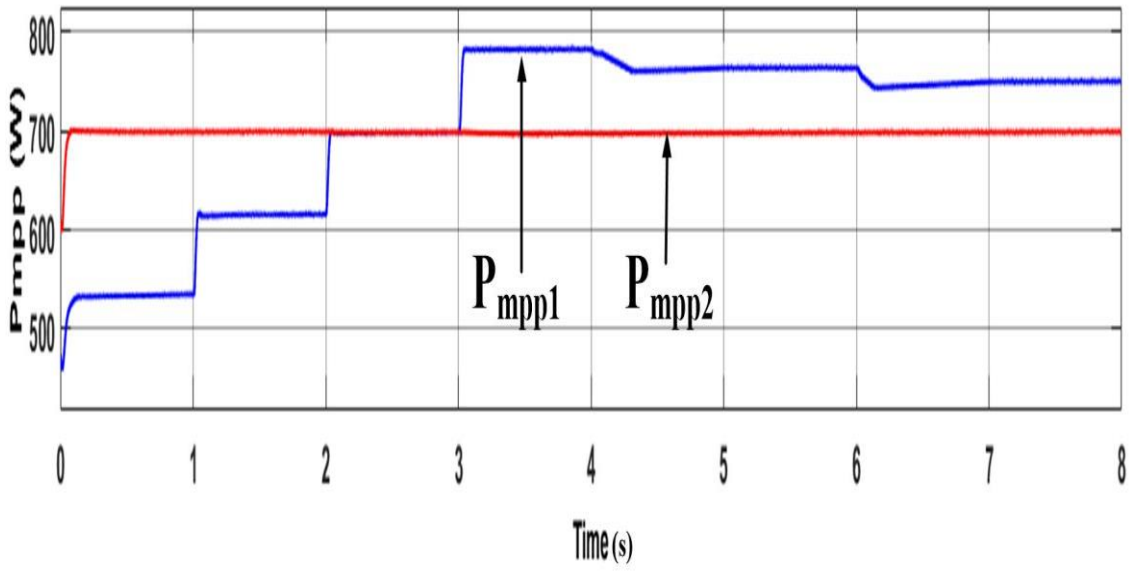

Fig. 5.8. Maximum Power (W) Extracted from PV_1 and PV_2.

The output parameters of grid current injected i_g, grid voltages and voltages across filter capacitors C_{o1} and C_{o2} are given below. The variations in grid current is similar to the PI controller with improved THD performance.

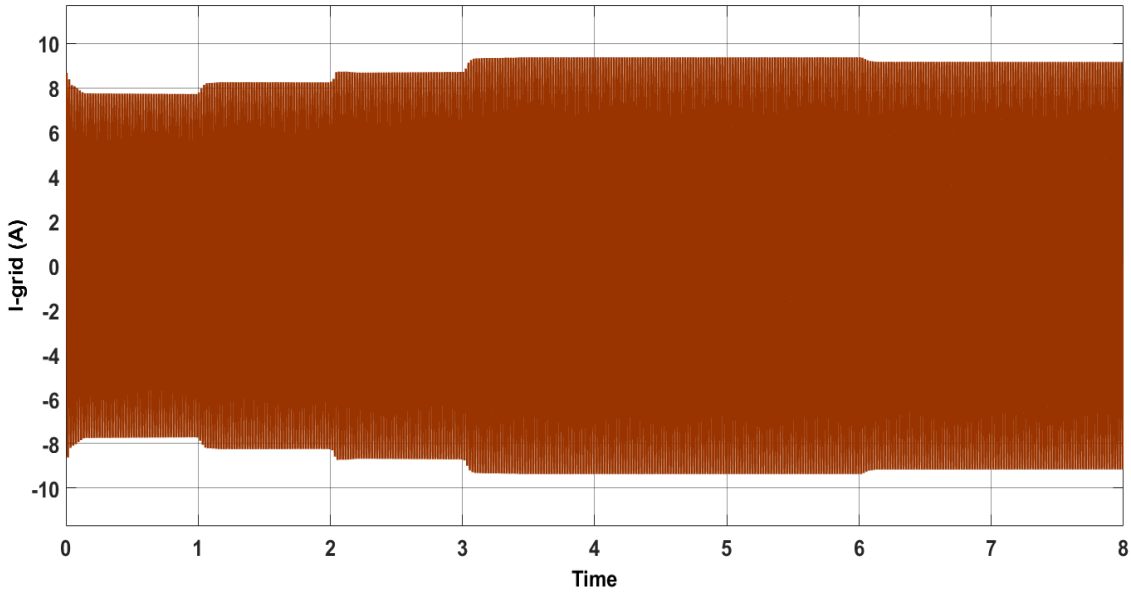

Fig. 5.9. Variation in Grid Current (i_g) in Amp

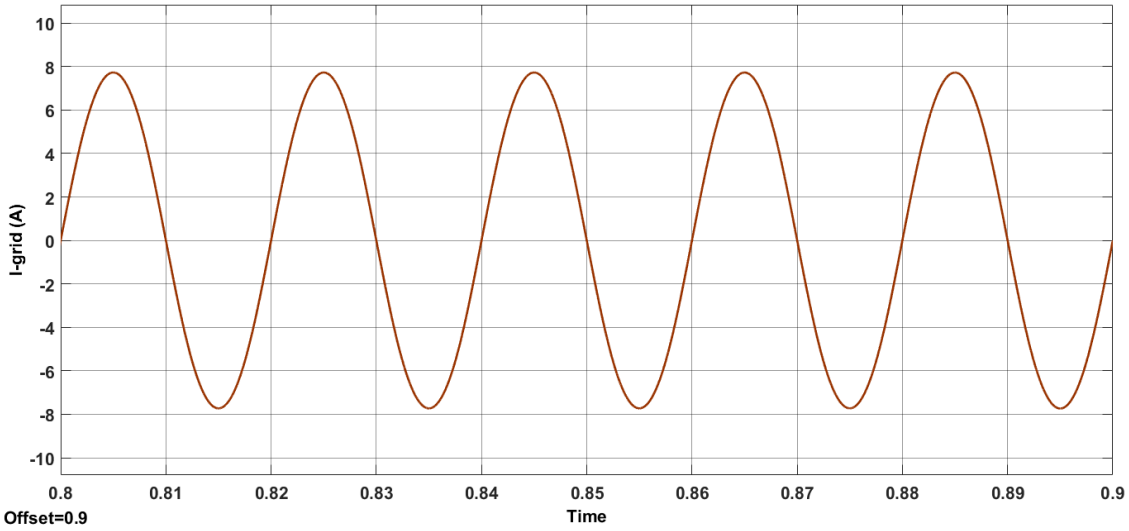

Fig. 5.10. Magnified Version of Grid Current i_g (A) for 5 cycles from t=0.8s to t=0.9s

From the above figure the FLC has slightly reduced the fluctuations with changing irradiance. For example in time t=3s the PI controller settles at t=3.5s and the FLC is smoother than the I controller with settling time of 0.1s. Hence it is concluded that the FLC is fast and performs better than the PI controller in terms settling time.

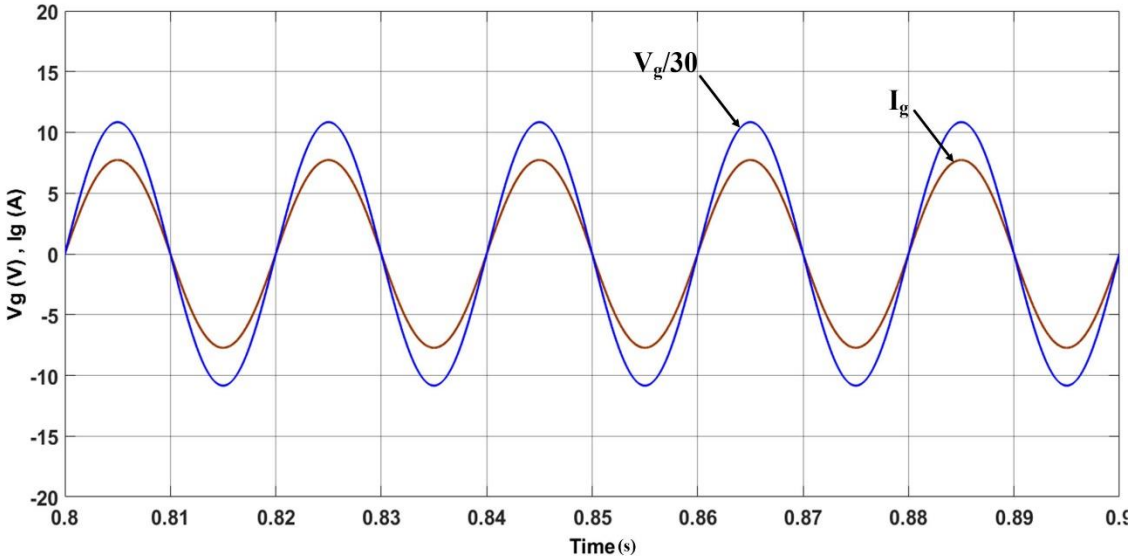

Fig. 5.11. Magnified Version of Grid Current i_g (A) and voltage v_g (V): t=0.8s to t=0.9s: FLC

Similar performance has been obtained for voltages across output filter capacitors C_{o1} and C_{o2} from PI controller.

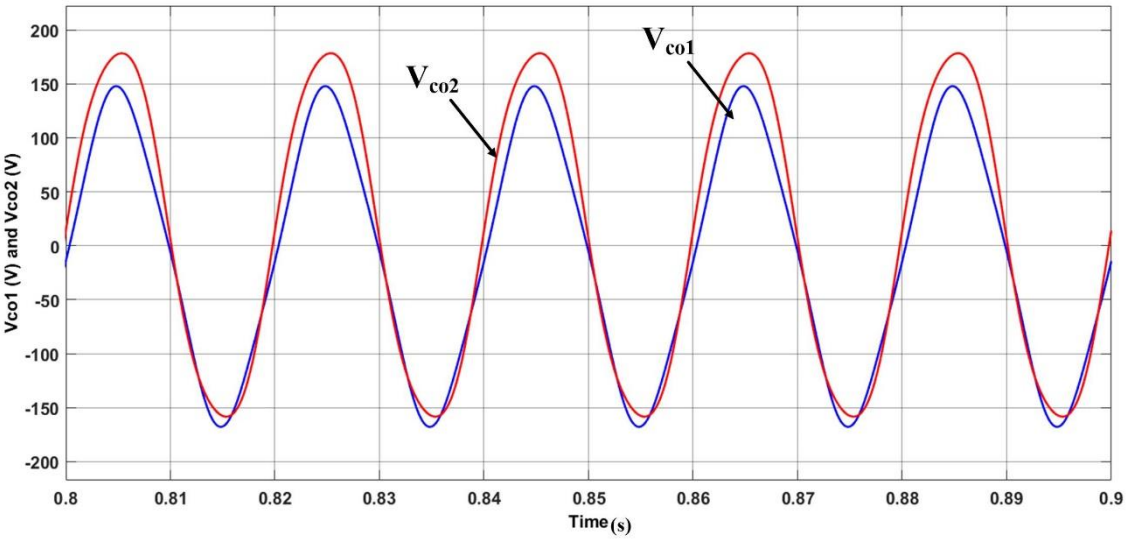

Fig. 5.12. Magnified Version of V_{co1} and V_{co2} for t=0.8s to t=0.9s: FLC

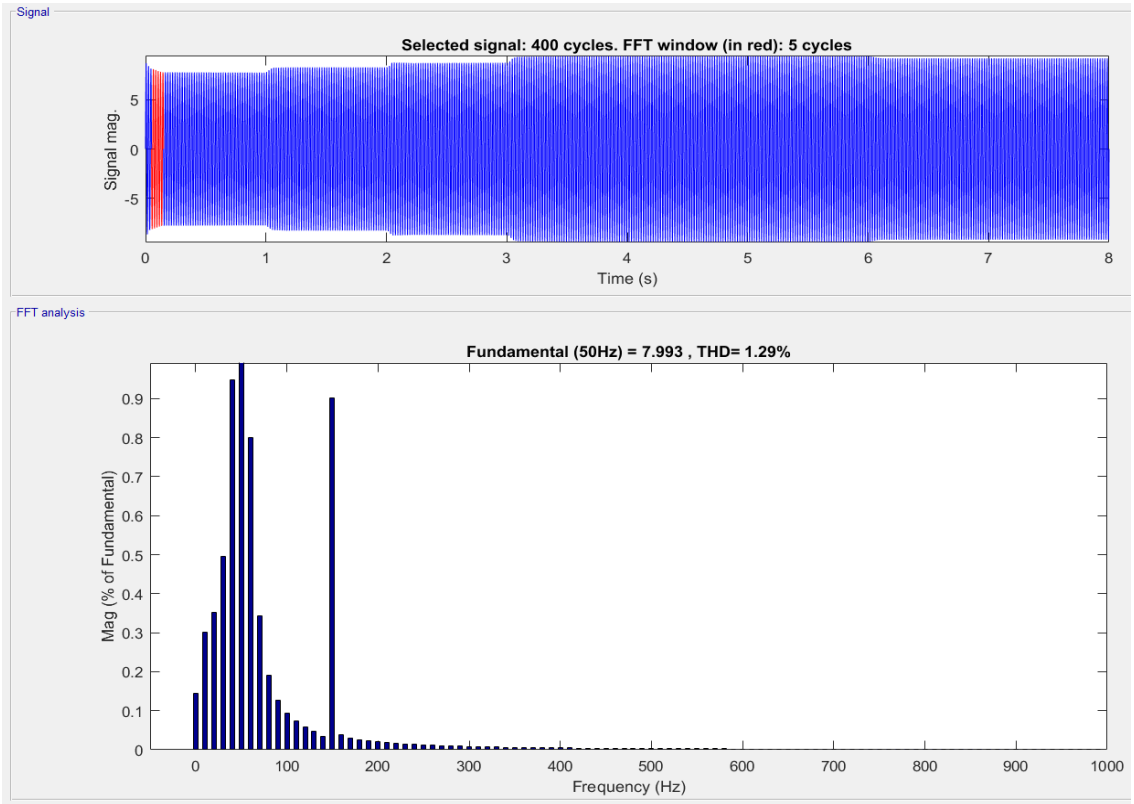

Fig. 5.13. THD% for injected grid current i_g taken for 5 cycles = 1.29%

5.4. CONCLUSION

In this chapter, the control scheme using the Fuzzy Logic Controller has been proposed. Similar results for input side DC quantities of maximum voltage, maximum current and maximum power extracted from the PV subarrays has been obtained. The output side results for the injected grid current and its THD% is also obtained and it is concluded that the THD% for the Fuzzy Logic Controller scheme is improved from the conventional PI controller.

It can be concluded from Fig.4.6 and Fig.5.6 that the control of the Vmpp1 is better in the case of fuzzy logic controller than the PI controller. At the instant t=3s when the irradiance is changed from 0.9 kW/m^2 to 1 kW/m^2 the voltage Vmpp1 is increased. In Fig.4.6 this increase in voltage has a transient time of 0.4s which has oscillations whereas in Fig.5.6 the change in voltage in smooth with a transient time of 0.1s. Similarly at t=4s and t=6s the fuzzy logic controller is able to control the Vmpp1 fast with less damping time and low oscillations. Hence the fuzzy logic controller increases the system damping

and improve the dynamic response with less transient oscillations. A comparative analysis of the two controllers is given in table 5.2.

	Injected Grid Current THD%	**Complexity**	**Tuning Required**	**Transient Oscillations**
Conventional PI Controller	5.74	High	Yes (Small Signal Analysis required for PI controller tuning)	High
Fuzzy Logic Controller	1.29	Low	No	Very Low

Table 5.2: Comparative Analysis of the Two Controllers

CHAPTER 6

CONCLUSION AND FUTURE WORK

6.1. CONCLUSION

Single stage transformerless grid tied inverter for PV applications has been simulated in this work. The single stage topologies are advantageous over the multi stage topologies since they have reduced weight, complexity and size. The work employs two serially connected PV panels and since the series connected modules are less the inverter is able to operate better under mismatched environmental conditions. The inverter is able to extract maximum power from both PV panels under varying atmospheric conditions. Simple Incremental Conductance MPPT algorithm has been used to reduce the complexity of the system. The operation of the inverter in positive and negative half cycles has been studied and the results are validated with the equations. The design criteria for the selection of passive elements of the system has also been taken into consideration.

The performance of the inverter has been compared using two control strategies with different controllers. A conventional PI controller and a Fuzzy Logic Controller has been used to compare the performance of the system. For the PI controller the small signal modelling has been studied and the frequency response is obtained to select the PI constants. For the Fuzzy Logic controller the controller has been derived and the if-lse ruling base system is also obtained and improved results from the PI controller has been obtained for the same.

The system performance, settling time, THD% for the injected grid current are some of the parameters where the two controllers has been compared. Table 6.1 depicts the comparison for the two controllers. The fuzzy logic controller performs better under

varying operating conditions than the conventional PI controller and also injects less harmonics into the grid through grid current. The settling time for the input side maximum extracted voltage is less for the FLC as shown in Table 6.1.

6.2. FUTURE WORK

In this work a grid tied inverter has been designed where the power supplied to the grid comes from two serially connected PV panels. This simulated model can be used to design the 1.5 KW hardware prototype which can be used to validate the simulation studies.

Further to increase the power rating of the system the serially connected modules can be increased and control strategies can be derived for the same to obtain useful results under varying operating and environmental conditions. Further investigations can be made using different intelligent controllers such as Proportional Resonant Controller and the results can be compared with the present work.

REFERENCES

[1] M. G. Villalva, J. R. Gazoli and E. R. Filho, "Comprehensive Approach to Modeling and Simulation of Photovoltaic Arrays," in *IEEE Transactions on Power Electronics*, vol. 24, no. 5, pp. 1198-1208, May 2009, doi: 10.1109/TPEL.2009.2013862.

[2] "Akshay Urja Magazine, March-April 2019, Volume 12, Issue 5," *Ministry of New and Renewable Energy*. [Online]. Available: https://mnre.gov.in/img/documents/uploads/0449bedb6afc4867b5b65c8ef9a22522.pdf. [Accessed: 12-Jun-2020].

[3] "National Solar Mission," *Wikipedia*, 10-Jul-2020. [Online]. Available: https://en.wikipedia.org/wiki/National_Solar_Mission. [Accessed: 19-Jun-2020].

[4] En.wikipedia.org. 2020. "*Financial Incentives For Photovoltaics"*. [online] Available at:https://en.wikipedia.org/wiki/Financial_incentives_for_photovoltaics#India. 2020].

[5] "Solar Parks," *Ministry of New and Renewable Energy*. [Online]. Available: https://mnre.gov.in/img/documents/uploads/bcf7e95e88ae4f8dbfa8bd25d21e5e12.pdf.

[6] "UDAY Scheme," *Ministry of Power*. [Online]. Available: https://www.uday.gov.in/home.php.

[7] S. Jain and V. Agarwal, "A Single-Stage Grid Connected Inverter Topology for Solar PV Systems With Maximum Power Point Tracking," in IEEE Transactions on Power Electronics, vol. 22, no. 5, pp. 1928-1940, Sept. 2007, doi: 10.1109/TPEL.2007.904202.

[8] F. S. Kang, S. Cho, S. J. Park, C. U. Kim, and T. Ise, "A new control scheme of a cascaded transformer type multilevel PWM inverter for a residential photovoltaic power conditioning system," Solar Energy, vol. 78, no. 6, pp. 727–738, 2005.

[9] T. J. Liang, Y. C. Kuo, and J. F. Chen, “Single-stage photovoltaic energy conversion system,” Proc. Inst. Elect. Eng., vol. 148, no. 4, pp. 339–344, 2001.

[10] Y. Chen and K. Ma-Smedley, “A cost-effective single-stage inverter with maximum power point tracking,” IEEE Trans. Power Electron., vol. 19, no. 5, pp. 1289–1294, Sep. 2004.

[11] F. Blaabjerg, Zhe Chen and S. B. Kjaer, "Power electronics as efficient interface in dispersed power generation systems," in *IEEE Transactions on Power Electronics*, vol. 19, no. 5, pp. 1184-1194, Sept. 2004, doi: 10.1109/TPEL.2004.833453.

[12] S. B. Kjaer, J. K. Pedersen, and F. Blaabjerg, “A review of single-phase grid-connected inverters for photovoltaic Modules,” IEEE Trans. Ind. Appl., vol. 41, no. 5, pp. 1292–1306, Sep./Oct. 2005.

[13] A. Luque and S. Hegedus, "The Physics of the Solar Cell," in Handbook of Photovoltaic Science and Engineering, Second Edition, Chichester, John Wiley & Sons, Ltd, 2011.

[14] S. Salivahanan, N. Suresh Kumar and A. Vallavaraj, "Semiconductor Diodes," in Electronic Devices and Circuits, Second Edition, New Delhi, Tata McGraw-Hill,2008, pp. 86-90.

[15] M. Boxwell, Solar Electricity Handbook: A Simple, Practical Guide to Solar Energy-Designing and Installing photovoltaic Solar Electric Systems, Warwickshire: Greenstream Publishing, 2012.

[16] A. K. Ghosh, C. Fishman and T. Feng, "Theory of the electrical and photovoltaic properties of polycrystalline silicon," Journal of Applied Physics, vol. 51, no. 1, p.446, 1980.

[17] G. Goodstal, "Photovoltaic Cells & Applications," in Electrical Theory for Renewable Energy, New York, Delmar, Cengage Learning, 2013, p. 155.

[18] M. Villalva, J. Gazoli and E. Filho, "Comprehensive Approach to Modelling and Simulation of Photovoltaic Arrays," IEEE Trans. Power Electron. vol. 24, no. 5, pp. 1198-1208, 2009.

[19] W. De Soto, S. A. Klein and W. A. Beckman, "Improvement and validation of a Model for photovoltaic array performance," Solar Energy, vol. 80, pp. 78-88, 2006.

[20] G. R. Walker, "Evaluating MPPT converter topologies using a matlab PV model," J.Elect. Electron. Eng., vol. 21, pp. 49-55, 2001.

[21] K. Ishaque, Z. Salam, H. Taheri and Syafaruddin, "Modelling and Simulation of Photovoltaic (PV) System during partial Shading based on a Two-diode Model," Simulation Modelling Practice and Theory, vol. 19, pp. 1613-1626, 2011.

[22] Manel Hlaili, Hfaiedh Mechergui, "Comparison of Different MPPT Algorithms with a Proposed One Using a Power Estimator for Grid Connected PV Systems", *International Journal of Photoenergy*, vol. 2016, Article ID 1728398, 10 pages, 2016. https://doi.org/10.1155/2016/1728398

[23] M. A. Elgendy, B. Zahawi, and D. J. Atkinson, "Assessment of perturb and observe MPPT algorithm implementation techniques for PV pumping applications," IEEE Transactions on Sustainable Energy, vol. 3, no. 1, pp. 21–33, 2012.

[24] H. Malek and Y. Chen, "BICO MPPT: a faster maximum power point tracker and its application for photovoltaic panels," International Journal of Photoenergy, vol. 2014, Article ID 586503, 9 pages, 2014.

[25] K. Visweswara, "An investigation of incremental conductance based maximum power point tracking for photovoltaic system," Energy Procedia, vol. 54, pp. 11–20, 2014.

[26] R. F. Coelho, F. M. Concer and D. C. Martins, "A MPPT approach based on temperature measurements applied in PV systems," *2010 IEEE International Conference on Sustainable Energy Technologies (ICSET)*, Kandy, 2010, pp. 1-6, doi: 10.1109/ICSET.2010.5684440.

[27] Islam M, Mekhilef S and Hasan M. "Single phase transformerless inverter topologies for grid-tied photovoltaic system - a review". Renew. Sustain. Energy Rev. 45, 69–86. doi.org-10.1016-j.rser.2015.01.009.

[28] Victor M, Greizer F, Bremicker S, and Hübler U, "Method of converting a direct current voltage from a source of direct current voltage, more specifically from a photovoltaic source of direct current voltage, into an alternating current voltage", ed:UnitedStatesPatents;2008.

[29] Z. Wang, F. Qi and Y. Wu, "High Efficient Single-phase Transformerless PV Inverter using GaN HEMTs and Si MOSFETs," *2019 IEEE Applied Power Electronics Conference and Exposition (APEC)*, Anaheim, CA, USA, 2019, pp. 3189-3194, doi: 10.1109/APEC.2019.8722265.

[30] Gonzalez R, Lopez J, Sanchis P and Marroyo L, "Transformerless inverter for single-phase photovoltaicsystems", IEEETransPowerElectron2007;22:693–7.

[31] Huafeng X, Shaojun X, Yang C and Ruhai H, “An optimized transformerless photo-voltaic grid-connected inverter”, IEEE Trans Ind Electron 2011; 58:1887–95.

[32] Gonzalez R, Gubia E,Lopez J and Marroyo L, “Transformerless single-phase multi-level-based photovoltaic inverter”, IEEE Trans Ind Electron 2008; 55:2694–702.

[33] Yunjie G, Wuhua L, Yi Z ,Bo Y, Chushan L and Xiangning H, “Transformerless inverter with virtual DC bus concept for cost-effective grid-connected PV power systems”, IEEE Trans Power Electron 2013; 28:793–805.

[34] S. V. Araujo, P. Zacharias, and R. Mallwitz, “Highly efficient single phase transformerless inverters for grid-connected photovoltaic systems,” IEEE Trans. Industrial Electronics, vol. 57, no. 9, pp. 3118-3128, Sep. 2010.

[35] T. Shimizu, O. Hashimoto, and G. Kimura, “A novel high-performance utility-interactive photovoltaic inverter system,” IEEE Trans. Power Electronics, vol. 18, no. 2, pp. 704-711, Mar. 2003.

[36] T. Shimizu, M. Hirakata, T. Kamezawa, and H. Watanabe, “Generation control circuit for photovoltaic modules,” IEEE Trans. Power Electronics, vol. 16, no. 3, pp. 293-300, May 2001.

[37] L. Zhang, K. Sun, L. Feng, H. Wu, and Y. Xing, “A Family of neutral point clamped full-bridge topologies for transformerless grid tied inverters,” IEEE Trans. Power Electronics, vol. 28, no. 2, pp. 730-739, Feb. 2013.

[38] S. Dutta, D. Debnath and K. Chatterjee, "A Grid-Connected Single-Phase Transformerless Inverter Controlling Two Solar PV Arrays Operating Under Different Atmospheric Conditions," in IEEE Transactions on Industrial Electronics, vol. 65, no. 1, pp. 374-385, Jan. 2018, doi: 10.1109/TIE.2017.2711577.

[39] I. Patrao, G. Garcera, E. Figueres, and R. Gonzalez-Medina, “Grid-tie inverter topology with maximum power extraction from two photovoltaic arrays,” IET Renewable Power Generation, vol. 8, no. 6, pp. 638-648, 2014.

[40] D. Debnath and K. Chatterjee, “Maximising power yield in a transformerless single phase grid connected inverter servicing two separate photovoltaic panels,” IET Renewable Power Generation, vol. 10, no. 8, pp. 1087-1095, 2016.

[41] Hoque, M. M., Hannan, M. A., Mohamed, A. Optimal algorithms for charge equalization controller of series connected lithium-ion battery cells in electric vehicle applications. IET Electrical Systems in Transportation 2017; 7(4): 267-277.

[42] Hannan, MA, Ghani, ZA, Mohamed, A, Uddin, MN. Real-Time Testing of a Fuzzy-Logic-Controller-Based Grid-Connected Photovoltaic Inverter System. IEEE Transactions on Industry Applications 2015; 51(6): 4775-4784.

[43] Zdenko, K, Stjepan, B. Fuzzy Controller Design-Theory and Applications. Florida: CRC Press, Taylor & Francis Group. 2006.

[44] Negnevitsky, M. Artificial Intelligence: A Guide to Intelligent System. Second Edition. England: Pearson Education Limited. 2005.

[45] Chaturvedi, DK. Modelling and Simulation of Systems Using MATLAB and Simulink. Florida: CRC Press. 2006.

[46] Mosalam, Hanan & Amer, Ragab & Morsy, G.A.. (2018). “Fuzzy logic control for a grid-connected PV array through Z-source-inverter using maximum constant boost control method.” Ain Shams Engineering Journal. 9. 10.1016/j.asej.2018.10.001.